






The deubiquitinase USP25 supports colonic inflammation and bacterial infection and promotes colorectal cancer

Xiao-Meng Wang^{1,2,3}, Ci Yang^{1,2,3}, Yin Zhao^{1,2} , Zhi-Gao Xu⁴, Wei Yang^{1,2,3}, Peng Wang^{1,2,3}, Dandan Lin⁵, Bin Xiong¹, Jing-Yuan Fang⁶, Chen Dong⁷ and Bo Zhong^{1,2,3}  

Bacterial infection or abnormal colonization in the gastrointestinal system is associated with subsets of inflammatory bowel disease and colorectal cancer. Here we demonstrated essential roles of ubiquitin-specific protease 25 (USP25) in experimental colitis, bacterial infections and colon cancer. Knockout or pharmacologic inhibition of USP25 potentiated immune responses after induction of experimental colitis or bacterial infections that promoted clearance of infected bacteria and resolution of inflammation and attenuated Wnt and SOCS3–pSTAT3 signaling, which inhibited colonic tumorigenesis. USP25 levels were positively or negatively correlated with *Fusobacterium nucleatum* colonization and β -catenin levels or SOCS3 levels in human colorectal tumor biopsies, respectively, and predicted poor prognosis of patients with cancers in the gastrointestinal system. Our findings suggest USP25 as a promoter and druggable target for gastrointestinal infections and cancers.

Inflammatory bowel disease (IBD) is a remitting and relapsing inflammatory disorder of the gastrointestinal (GI) tract characterized by pain, diarrhea and bloody stools and comprises two primary diseases: Crohn's disease and ulcerative colitis¹. Genome-wide association studies and gut microbiome analyses have identified various susceptible single-nucleotide polymorphisms and implicated imbalance of protective and pathogenic bacteria in patients with IBD^{2,3}. For example, nucleotide binding oligomerization domain containing 2 (NOD2) is required for antibacterial immune responses and mutations of NOD2 are associated with IBD susceptibility^{4–7}. A depletion of bacteria with anti-inflammatory effects such as *Faecalibacterium prausnitzii* and colonization of proinflammatory bacteria, including adherent-invasive *Escherichia coli* and *Fusobacterium varium* are correlated with and potentially contribute to IBD^{8–10}.

Colorectal cancer (CRC) is the third most prevalent cancer and the second-leading cause of cancer-related deaths worldwide with an estimated new diagnosis of 1.8 million patients and 880,000 deaths in 2018 (ref. 11). The development of CRC involves the accumulation of genetic alterations during repeated rounds of inflammation and mucosal healing that facilitate the evolution and malignancy of preneoplastic clones and excessive activation of STAT3 in intestinal epithelial cells by repeated infection-caused proinflammatory factor stimulation that promotes malignant cell survival¹². The Cancer Genome Atlas projects have identified a number of frequently mutated genes or pathways associated with CRC, including Wnt signaling pathway, *KRAS* and *TP53*, which have been confirmed with various mouse colon cancer models^{13–16}, indicating that targeting the components involved in these pathways would provide plausible therapeutic strategies.

Host pattern-recognition receptors (PRRs) recognize microbial pathogen-associated molecular patterns to initiate innate immune

responses against invading pathogens¹⁷. PRRs and PRR-mediated signaling play essential roles in colitis or colon cancer¹⁸. For example, Toll-like receptor (TLR)4 senses lipopolysaccharide (LPS) in the cell wall of Gram-negative bacteria and triggers MyD88- and TRIF-dependent signaling. Ectopic expression of TLR4 in the epithelia or deficiency of *Tlr4* or *Myd88* in mice results in hyper-sensitivity to chemically induced colitis, which is associated with dysbiotic microbiota and bacterial invasion in the mucosa^{19–21}. We have previously shown that USP25 inhibits TLR-triggered MyD88-mediated inflammatory cytokine induction by deubiquitinating and stabilizing tumor necrosis factor (TNF) receptor associated factor 3 (TRAF3)^{22,23}. In addition, USP25 promotes Wnt signaling and cell growth by deubiquitinating and stabilizing tankyrases *in vitro*²⁴. Whether and how USP25 regulates bacterial infections, infection-associated colitis as well as Wnt-related biological processes *in vivo* has not been investigated.

In this study, we discovered that USP25 deficiency results in hyper-immune responses after dextran sulfate sodium (DSS) treatment or *Citrobacter rodentium* or *Salmonella enterica* Typhimurium (ST) infection. Meanwhile, knockout of USP25 downregulates Wnt signaling and modulates the SOCS3–pSTAT3 axis and thereby inhibits tumorigenesis in the colon. Finally, pharmacologic inhibition of USP25 alleviates DSS-induced colitis, protects from bacterial infections and impairs colon cancer development. These findings collectively suggest critical roles of USP25 in colitis and CRC, which serves as a potential therapeutic target.

Results

USP25 deficiency in nonhematopoietic cells leads to resistance to DSS-induced colitis. In our immunoblot and immunohistochemistry

¹Department of Gastrointestinal Surgery, Medical Research Institute, Zhongnan Hospital of Wuhan University, Wuhan, China. ²Frontier Science Center for Immunology and Metabolism, Wuhan University, Wuhan, China. ³Department of Virology, College of Life Sciences, Wuhan University, Wuhan, China. ⁴Institute of Hepatobiliary Diseases, Transplant Center, Hubei Key Laboratory of Medical Technology on Transplantation, Zhongnan Hospital of Wuhan University, Wuhan, China. ⁵Cancer Center, Renmin Hospital of Wuhan University, Wuhan, China. ⁶Division of Gastroenterology and Hepatology, Renji Hospital, School of Medicine, Shanghai Jiao Tong University, Shanghai, China. ⁷Institute for Immunology and School of Medicine, Tsinghua University, Beijing, China. ✉e-mail: zhongbo@whu.edu.cn

(IHC) assays, we found that USP25 was expressed ubiquitously in the stomach, small intestine and colon as well as in the crypt of the small intestine and in epithelial cells (ECs) and lamina propria mononuclear cells (LPMCs) of the colon (Fig. 1a,b), consistently with recent single-cell RNA-sequencing (scRNA-seq) results that *Usp25* is ubiquitously expressed in various types of cells in the intestine^{25,26}. We further found that the numbers of Paneth cells (lysozyme⁺) in the crypts and the number of goblet cells (AB/PAS⁺) in the villi were significantly increased in the small intestines of *Usp25*^{-/-} mice compared to *Usp25*^{+/+} mice (Fig. 1c). Ki67 and SOX9 staining was slightly decreased in *Usp25*^{-/-} crypts compared to the *Usp25*^{+/+} counterparts, although the difference did not reach statistical significance (Fig. 1c). Together, these data suggest that USP25 is ubiquitously expressed and inhibits differentiation of secretory cells in the intestine.

We next induced a DSS-colitis model with *Usp25*^{+/+} and *Usp25*^{-/-} mice and observed that *Usp25*^{-/-} mice exhibited increased resistance to weight loss, diarrhea and colon shortening compared to the controls (Fig. 1d)²⁷. Hematoxylin and eosin (H&E) staining of the colons showed that *Usp25*^{-/-} mice had more leukocyte infiltration and more remaining epithelium than the *Usp25*^{+/+} mice (Fig. 1e). USP25 has been shown to promote type I interferon (IFN) induction^{22,23}. However, *Usp25*^{-/-}*Ifnar1*^{-/-} mice were also more resistant to DSS-induced colitis than *Ifnar1*^{-/-} mice as monitored by weight loss, colon length and H&E staining of colons (Extended Data Fig. 1a–c). These data suggest that USP25 promotes colitis in a manner independently of type I IFN signaling.

Analysis of LPMCs in the colon suggested more leukocytes, CD11b⁺F4/80⁺ macrophages and CD8⁺ T cells and fewer CD11b⁺Gr-1⁺ neutrophils and CD4⁺interleukin (IL)-17A⁺ T cells infiltrating in colon lamina propria of *Usp25*^{-/-} and *Usp25*^{-/-}*Ifnar1*^{-/-} mice than in *Usp25*^{+/+} or *Ifnar1*^{-/-} mice after DSS treatment, respectively (Extended Data Fig. 1d–i). To determine whether such a difference was due to a defect of USP25 in immune cells, we adoptively transferred *Usp25*^{+/+} or *Usp25*^{-/-} bone marrow cells (CD45.2⁺) into irradiated CD45.1⁺ congenic mice followed by DSS treatment (Extended Data Fig. 2a). Results from flow cytometry analysis suggested that the total cell numbers and the percentages of different immune cells were comparable in the colon lamina propria of CD45.1⁺ mice receiving either *Usp25*^{+/+} or *Usp25*^{-/-} bone marrow cells (Extended Data Fig. 2b–d), indicating that hematopoietic deficiency of USP25 does not affect immune cell homeostasis or differentiation in DSS-induced colitis. Consistently with this notion, we found that irradiated *Usp25*^{-/-} mice receiving either *Usp25*^{+/+} or *Usp25*^{-/-} bone marrow cells were more resistant to DSS-induced colitis than irradiated *Usp25*^{+/+} mice receiving either wild-type or *Usp25*^{-/-} bone marrow cells as monitored by weight loss, colon length and H&E staining of colons and that DSS treatment induced upregulation of USP25 in colon ECs (Fig. 1f–h and Extended Data Fig. 2e). These results indicate that USP25 deficiency in nonhematopoietic cells plays a dominant role

in the resistance of DSS-induced colitis and homeostasis of immune cells in colon lamina propria.

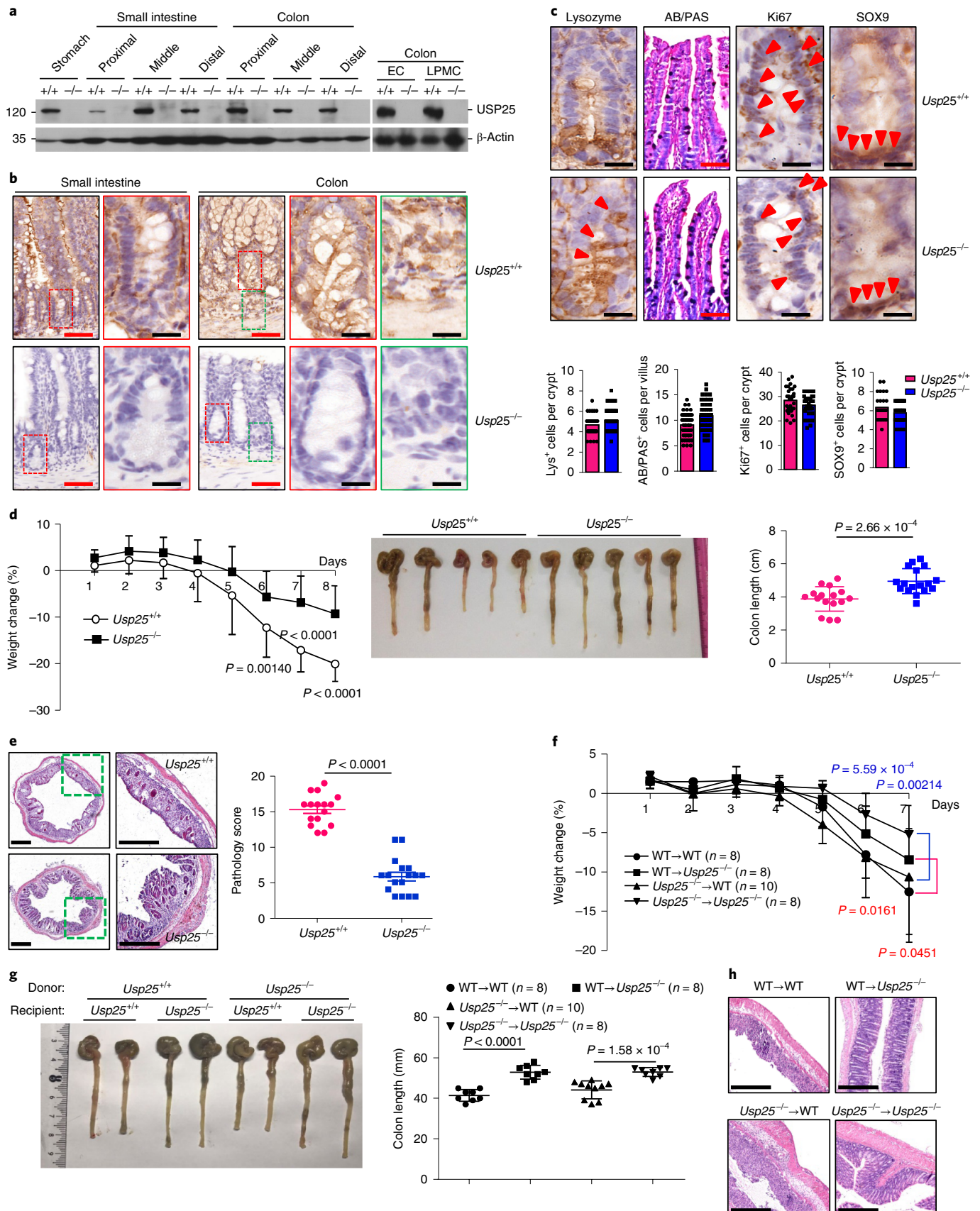
USP25 deficiency alters cytokine expression in DSS-treated colon. Results from transcriptome analysis of colons from DSS-treated *Usp25*^{-/-} and *Usp25*^{+/+} mice suggested that 878 genes (529 downregulated and 349 upregulated) were differentially expressed with statistical significance, which were closely related to cytokine and cytokine receptor interaction and bacterial or viral infections (Fig. 2a,b and Supplementary Table 1). Gene-set enrichment analysis (GSEA) characterized differentially expressed genes into three clusters of cytokines and chemokines, IFN-regulated factor (IRF)-dependent products and genes with antibacterial activities (Fig. 2c and Supplementary Table 2). Results from quantitative reverse transcription (qRT)-PCR analysis confirmed that expression of proinflammatory cytokines and chemokines and genes related to acute-phase response to bacterial infection was significantly higher and expression of IRF- or IFN-dependent genes was significantly lower in *Usp25*^{-/-} or *Usp25*^{-/-}*Ifnar1*^{-/-} colons than in *Usp25*^{+/+} or *Ifnar1*^{-/-} colons during DSS-induced colitis, respectively (Fig. 2d–f and Extended Data Fig. 3a–c). Consistently with these observations, levels of phosphorylated p65 and p38 were potentiated and levels of TRAF3 were decreased in colon tissues from *Usp25*^{-/-} mice compared to *Usp25*^{+/+} mice after a 2-d DSS treatment and in LPS- or peptidoglycan (PGN)-treated *Usp25*^{-/-} colon organoids compared to the *Usp25*^{+/+} colon organoids (Fig. 2g,h), which prompted us to hypothesize that USP25 deficiency-mediated protection of colitis was related to commensal bacteria in the GI tract. In support of this notion, knockout of USP25 did not show any protection from mortality, weight loss or colon shortening after antibiotic treatment followed by DSS induction (Extended Data Fig. 2e–g). Expression of related genes was comparable between *Usp25*^{-/-} and *Usp25*^{+/+} colons (Extended Data Fig. 2h). These data suggest that USP25 deficiency alters gene expression in DSS-treated colons and protects mice from DSS-induced colitis in a manner dependent on commensal bacteria.

***Usp25*^{-/-} mice exhibit hyper-immune responses to bacterial infections.** DSS treatment induces epithelium damage, which allows commensal bacteria invasion and infection and thereby induces severe inflammation in the GI tract. To investigate whether USP25 regulates antibacterial infections in the GI tract, we infected mice with *Citrobacter rodentium* and monitored body weight and fecal bacteria count. As shown in Fig. 3a,b, *Usp25*^{-/-} mice had more constant gain of weight than *Usp25*^{+/+} mice and the fecal bacteria count of *Usp25*^{-/-} mice was 2–4 logs lower than that of *Usp25*^{+/+} mice, indicating that USP25 promotes bacterial replication in vivo. The spleens and colons of *Usp25*^{-/-} mice were heavier and longer than those of *Usp25*^{+/+} mice at day 16 after oral challenge of *C. rodentium* (Fig. 3c,d). There were significantly more numbers of

Fig. 1 | USP25 deficiency leads to resistance to DSS-induced colitis. **a**, Immunoblot analysis of USP25 in stomach, proximal, middle and distal small intestine and colon and in the ECs or the LPMCs of colon. **b**, IHC analysis of USP25 in small intestines and colons of *Usp25*^{+/+} and *Usp25*^{-/-} mice. Red and green rectangles indicate crypts and lamina propria, respectively. **c**, IHC analysis (upper images) and counts (lower graphs) of lysozyme (lys) ($n=50$ crypts from three mice), AB/PAS ($n=50$ villi from three mice), Ki67 ($n=30$ crypts from three mice) or SOX9 ($n=30$ crypts from three mice) staining of crypts or villi of small intestines of *Usp25*^{+/+} and *Usp25*^{-/-} mice. Arrow heads indicate positive staining. **d**, Body weight change (left) and gross morphological change and lengths of colons (right) of *Usp25*^{+/+} ($n=16$) and *Usp25*^{-/-} ($n=17$) mice that were given 2.5% DSS in drinking water for 5 d, followed by normal drinking water for another 3 d. **e**, Images (left) and pathological scores (right) of H&E-stained colon sections of *Usp25*^{+/+} ($n=16$) and *Usp25*^{-/-} ($n=17$) mice in **d**. **f,g**, Body weight change (**f**) and gross morphological change and lengths of colons (**g**) of the indicated chimeric mice (wild-type (WT) → WT ($n=8$ mice), WT → *Usp25*^{-/-} ($n=8$ mice), *Usp25*^{-/-} → WT ($n=10$ mice), *Usp25*^{-/-} → *Usp25*^{-/-} ($n=8$ mice)) that were given 2.5% DSS in drinking water for 5 d, followed by normal drinking water for another 2 d. **h**, Images of H&E-stained colon sections of the indicated chimeric mice in **f**. Statistical analyses were performed with two-tailed Student's *t*-test (**d–g**). Red and black scale bars, 100 μ m and 20 μ m (in **b,c**), respectively. Scale bars, 0.4 mm (in **e,h**). Data are representative of two independent experiments (**a–c**) or a combination of four (**d,e**) or two (**f–h**) independent experiments (mean in **c** and mean \pm s.d. in **d–g**). Uncropped immunoblot images and numerical source data for the experiments in this figure are in Source Data Fig. 1.

total cells and more numbers and higher percentages of activated CD8⁺ T cells (CD44⁺CD62L⁻) and FAS⁺GL7⁺ germinal center B cells in spleens from *Usp25*^{-/-} mice than in those from *Usp25*^{+/+}

mice after 14 d of *C. rodentium* infection (Extended Data Fig. 4a–c). H&E and immunofluorescent staining showed attenuated inflammation and impaired *C. rodentium* replication in colons of *Usp25*^{-/-}



mice compared to *Usp25^{+/+}* mice (Fig. 3e). Consistently with these observations, the expression of proinflammatory cytokines and antibacterial peptides was significantly higher in infected colons of *Usp25^{-/-}* mice than in those of *Usp25^{+/+}* mice (Fig. 3f). In addition, increased levels of phosphorylated p65 and p38, decreased levels of TRAF3 and higher levels of TNF- α and IL-6 were observed in colon tissues or sera from *Usp25^{-/-}* mice compared to *Usp25^{+/+}* mice at day 5 or 9 after *C. rodentium* infection, respectively (Fig. 3g,h).

In addition, *Usp25^{-/-}* mice were more resistant to ST-induced weight loss and death and bacteria count was significantly decreased in the feces of *Usp25^{-/-}* mice compared to *Usp25^{+/+}* mice (Fig. 3i–k). Expression of proinflammatory cytokines was significantly higher in colons of *Usp25^{-/-}* mice than in those of *Usp25^{+/+}* mice after ST infection (Fig. 3l). Consistently with these observations, increased levels of phosphorylated p65 and p38, TNF- α and IL-6 were observed in colon tissues and sera from *Usp25^{-/-}* mice compared to *Usp25^{+/+}* mice at day 3 and 6 after ST infection, respectively (Fig. 3m,n). In contrast, the expression of IRF/IFN-dependent genes was lower in colons of *Usp25^{-/-}* mice or colon organoids than in those of *Usp25^{+/+}* mice or organoids after *C. rodentium* or ST infection or LPS treatment (Fig. 3o and Extended Data Fig. 4d–g). These findings collectively suggest that USP25-deficient mice exhibit hyper-immune responses to bacterial infections and thereby restrict inflammation and bacterial infections.

Previous studies have demonstrated critical roles of *Fusobacterium* in IBD and CRC development and chemoresistance^{10,28–32}. Notably, the levels of USP25 were higher in human CRC biopsies with *F. nucleatum* colonization than in those without and positively correlated with the intensities of *F. nucleatum* colonization (Extended Data Fig. 4h,i and Supplementary Table 3), indicating that USP25 expression and bacterial colonization might be mutually promoted during inflammation or tumorigenesis. In this context, we have found that expression of USP25 was significantly upregulated in colon tissues after DSS treatment, *C. rodentium* or ST infection and in colon organoids after *C. rodentium* or ST infection or LPS stimulation (Fig. 2f,g and Extended Data Fig. 4f,g,j,k). In an *F. nucleatum*-induced *Apc^{Min/+}* colon cancer mouse model³¹, we found that ablation of USP25 in *Apc^{Min/+}* mice significantly impaired tumorigenesis in the colon after *F. nucleatum* infection and inhibited *F. nucleatum* colonization in colon tumors (Extended Data Fig. 4l–n). Collectively, these data suggest that USP25 suppresses immune responses against bacterial infection and thereby promotes bacteria replication and inflammation.

USP25 promotes intestinal tumorigenesis. As analysis of the transcriptome data suggested critical roles of USP25 in the expression of proinflammatory cytokines, *Socs3* and Wnt-related genes (Figs. 2 and 3 and data described below), we extended our investigations to determine whether USP25 regulates intestinal tumorigenesis. Analysis of Gene Expression Profiling Interactive Analysis (GEPIA) data suggested that the expression levels of USP25 were associated with poor overall survival of patients with colon, rectum and stomach adenocarcinoma (gepia.cancer-pku.cn) (Extended Data Fig. 5a), indicating a correlation of USP25 and GI tract

cancers. In the azoxymethane (AOM)/DSS model of colon cancer, we observed less tumor incidence and reduced tumor numbers in the colons of female *Usp25^{-/-}* mice compared to *Usp25^{+/+}* mice (Fig. 4a). In addition, male *Usp25^{-/-}* mice were more resistant to lethality than *Usp25^{+/+}* mice during AOM/DSS induction (Fig. 4b). In the AOM/*Vil-Cre;Trp53^{fl/fl}* (VP) model, knockout of USP25 significantly reduced tumor numbers in colons and promoted survival of mice (Fig. 4c,d). In a third model of intestinal cancer, ablation of USP25 in *Apc^{Min/+}* mice significantly inhibited tumorigenesis in the colon and small intestine (Fig. 4e,f). Consistently, knockout of USP25 promoted survival of *Apc^{Min/+}* mice (Fig. 4g). In addition, levels of USP25 were higher in tumor tissues than in normal tissues from the same mice or from control mice of the same age (Extended Data Fig. 5b), indicating that upregulation of USP25 was accompanied with tumorigenesis in the colon. These data together suggest that USP25 supports colon cancer development in multiple mouse models.

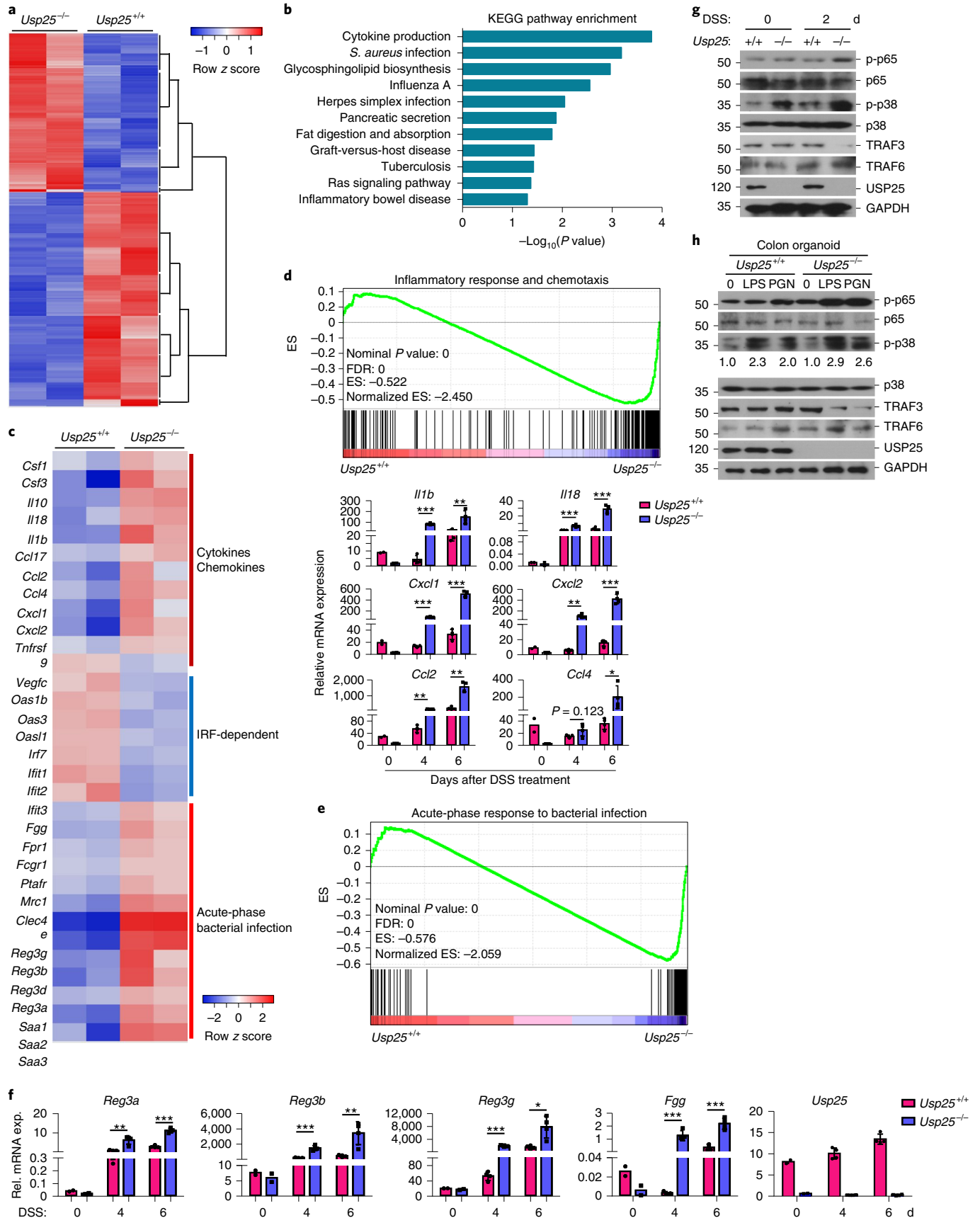
USP25 promotes Wnt signaling and inhibits SOCS3 expression. It has been shown that proinflammatory cytokines are involved in tumorigenesis in these models^{14,15,33}. However, we found comparable levels of proinflammatory cytokines in *Usp25^{+/+}* and *Usp25^{-/-}* colon tumors from the AOM/DSS, AOM/VP or *Apc^{Min/+}* models (Extended Data Fig. 5c–f). In contrast, the expression of Wnt pathway genes was significantly reduced in *Usp25^{-/-}* colons or colon organoids compared to that in *Usp25^{+/+}* counterparts after DSS treatment, bacterial infection or Wnt3a stimulation (Fig. 5a–d and Extended Data Fig. 5g,h), consistently with a recent report that USP25 promotes Wnt signaling²⁴. In addition, the products of Wnt-related genes were lower in USP25-deficient colons or small intestine tumor tissues than in USP25-sufficient counterparts (Fig. 5e and Extended Data Fig. 5i–k), suggesting that USP25 regulates Wnt signaling during colonic tumorigenesis.

In contrast to downregulated Wnt signals, SOCS3 was significantly upregulated in USP25-deficient tissues compared to USP25-sufficient counterparts during DSS treatment or colon cancer induction (Fig. 5a–e and Extended Data Fig. 5i–k). Notably, upregulation of *Socs3* in *Usp25^{-/-}* versus *Usp25^{+/+}* organoids was observed by *C. rodentium* or ST infection but not by LPS treatment (Extended Data Fig. 4f,g) and depletion of bacteria in the GI tract by antibiotics diminished the differences of *Socs3* expression between *Usp25^{-/-}* and *Usp25^{+/+}* colons after DSS treatment (Extended Data Fig. 3h), indicating that USP25 restricts SOCS3 induction dependently on gut bacteria but independently of its regulation of LPS-triggered signaling. SOCS3 plays a negative regulatory role in STAT3 activation, colitis and CRC development^{34,35}. Expectedly, phosphorylation of STAT3 was impaired in USP25-deficient colon or small intestine tumors compared to USP25-sufficient counterparts after tumor induction (Fig. 5e and Extended Data Fig. 5i–k). In addition, USP25 levels were positively or negatively correlated with β -catenin and pSTAT3 or SOCS3 levels in human CRC biopsies, respectively (Extended Data Fig. 6a,b). These results suggest that USP25 promotes Wnt signaling and STAT3 activation, which are hallmarks for tumorigenesis in the GI tract.

Fig. 2 | USP25 deficiency leads to altered cytokine expression. **a,b**, Heat map (**a**) and KEGG pathway enrichment analysis (**b**) of the transcriptome of colon tissues from *Usp25^{+/+}* ($n = 2$) and *Usp25^{-/-}* ($n = 2$) mice that were given 2.5% DSS in drinking water for 5 d, followed by normal drinking water for another 2 d. *S. aureus*, *Staphylococcus aureus*. **c**, Heat map of selected genes related to inflammatory cytokines and chemokines, IRF-dependent genes and acute-phase bacterial infection. **d–f**, GSEA and qRT-PCR analysis of related genes of colon tissues from *Usp25^{+/+}* ($n = 2, 4$ and 4 at day 0, 4 and 6, respectively) and *Usp25^{-/-}* ($n = 2, 4$ and 4 at day 0, 4 and 6, respectively) mice that were given 2.5% DSS in drinking water for indicated time points. ES, enrichment score; NES, nonenrichment score; FDR, false discovery rate. **g,h**, Immunoblot analysis of indicated proteins in colon tissues from *Usp25^{+/+}* and *Usp25^{-/-}* mice that were given 2.5% DSS in drinking water for 0–2 d (**g**) or in *Usp25^{+/+}* and *Usp25^{-/-}* colon organoids that were left untreated or stimulated with LPS ($10 \mu\text{g ml}^{-1}$) or PGN ($10 \mu\text{g ml}^{-1}$) for 30 min (**h**). * $P < 0.05$; ** $P < 0.01$; *** $P < 0.001$ (hypergeometric test in **b**; two-way analysis of variance (ANOVA) in **d,f**). Data are representative of two independent experiments (**d–h**) (mean \pm s.d. in **d,f**). Uncropped immunoblot images and numerical source data for the experiments in this figure can be found in Source Data Fig. 2.

Targeting USP25 attenuates DSS-induced colitis and restricts bacterial infections. We next synthesized the compound AZ, which has been demonstrated as a potent inhibitor of USP25 activity and

examined whether AZ1 could prevent development of related diseases (Extended Data Fig. 6c,d)³⁶. Gavage of AZ1 did not affect weight gain, sizes or weight of spleen and peripheral lymph nodes of



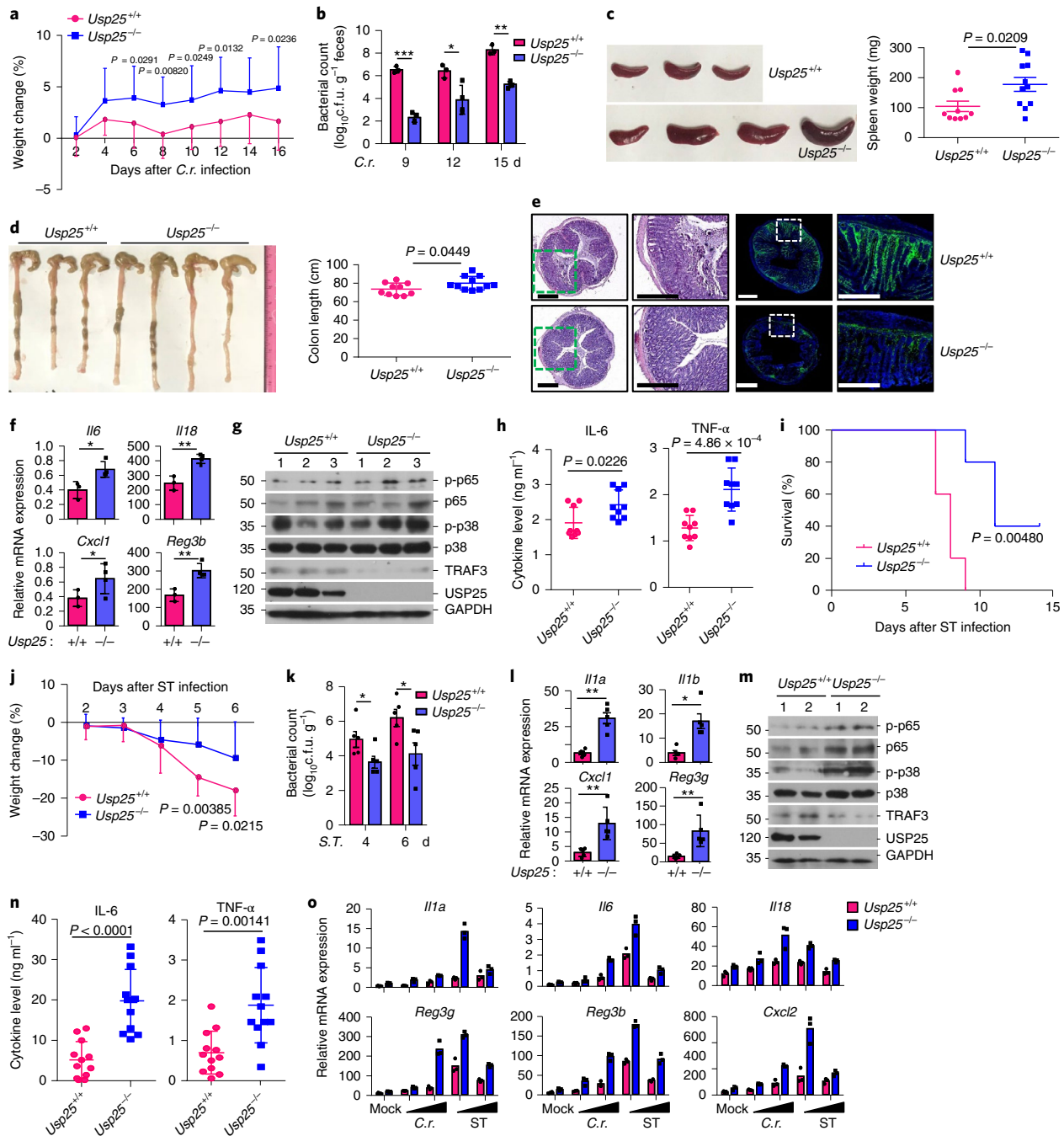


Fig. 3 | *Usp25*^{-/-} mice exhibit resistance to bacterial infections. **a**, Body weight change of *Usp25*^{+/+} ($n=10$) and *Usp25*^{-/-} ($n=11$) mice that were injected with 1×10^9 colony-forming units (c.f.u.) of *C. rodentium* by gavage. C.r., *C. rodentium*. **b**, Bacterial counts of *Usp25*^{+/+} ($n=3$) and *Usp25*^{-/-} ($n=4$) mice at 9, 12 or 15 d after injection of *C. rodentium* (1×10^9 c.f.u.) by gavage. **c,d**, Spleen morphological change and weights (**c**) and colon morphological change and lengths (**d**) of *Usp25*^{+/+} ($n=10$) and *Usp25*^{-/-} ($n=11$) mice 16 d after *C. rodentium* infection. **e,f**, Images of H&E-stained colon sections (left two columns) and immunofluorescence staining (with anti-*C. rodentium*) of colon sections (**e**) and qRT-PCR analysis of *Il6*, *Il18*, *Cxcl1* and *Reg3b* (**f**) in colons of *Usp25*^{+/+} ($n=3$) and *Usp25*^{-/-} ($n=4$) mice 16 d after *C. rodentium* infection. **g**, Immunoblot analysis of indicated proteins in colon tissues from *Usp25*^{+/+} ($n=3$) and *Usp25*^{-/-} ($n=3$) mice 5 d after *C. rodentium* infection (1×10^9 c.f.u.). **h**, ELISA analysis of indicated inflammatory cytokines levels in sera of *Usp25*^{+/+} ($n=9$) and *Usp25*^{-/-} ($n=9$) mice 9 d after *C. rodentium* infection (1×10^9 c.f.u.). **i**, Survival of *Usp25*^{+/+} ($n=10$) and *Usp25*^{-/-} mice ($n=10$) that were injected with ST (SL1344) (1×10^7 c.f.u.) by gavage and monitored for 14 d. **j**, Body weight change of *Usp25*^{+/+} ($n=10$) and *Usp25*^{-/-} mice ($n=9$) that were injected with ST (5×10^6 c.f.u.) by gavage. **k,l**, Bacterial counts in fecal homogenates (**k**) and qRT-PCR analysis of colons of *Usp25*^{+/+} and *Usp25*^{-/-} mice ($n=5$) that were injected with ST (5×10^6 c.f.u.) by gavage and monitored for 6 d (**l**). **m**, Immunoblot analysis of indicated proteins in colon tissues from *Usp25*^{+/+} ($n=2$) and *Usp25*^{-/-} ($n=2$) mice 3 d after ST (5×10^6 c.f.u.) infection. **n**, ELISA analysis of indicated inflammatory cytokines levels in the sera of *Usp25*^{+/+} ($n=9$) and *Usp25*^{-/-} ($n=9$) mice 6 d after ST (5×10^6 c.f.u.) infection. **o**, qRT-PCR analysis of *Il1a*, *Il6*, *Il18*, *Reg3b*, *Reg3g* and *Cxcl2* in *Usp25*^{+/+} ($n=3$, technical replicates) and *Usp25*^{-/-} colon organoids ($n=3$, technical replicates) infected with *C. rodentium* (1×10^7 c.f.u.) or ST (5×10^6 c.f.u.) for 1 h. * $P < 0.05$; ** $P < 0.01$; *** $P < 0.001$ (two-way ANOVA in **b** and **k**, two-tailed Student's *t*-test in **a,c,d,f,h,j,l** and **n** or log-rank analysis in **i**). Scale bars, 0.4 mm (**e**). Data are combined of three (**a,c,d**) or two (**h-j,n**) independent experiments or representative of three (**b,f**) or two (**g,h,k-m,o**) independent experiments (mean in **o** and mean \pm s.d. in **a-d,f,h,j-l** and **n**). Uncropped immunoblot images and numerical source data for the experiments in this figure are in Source Data Fig. 3.

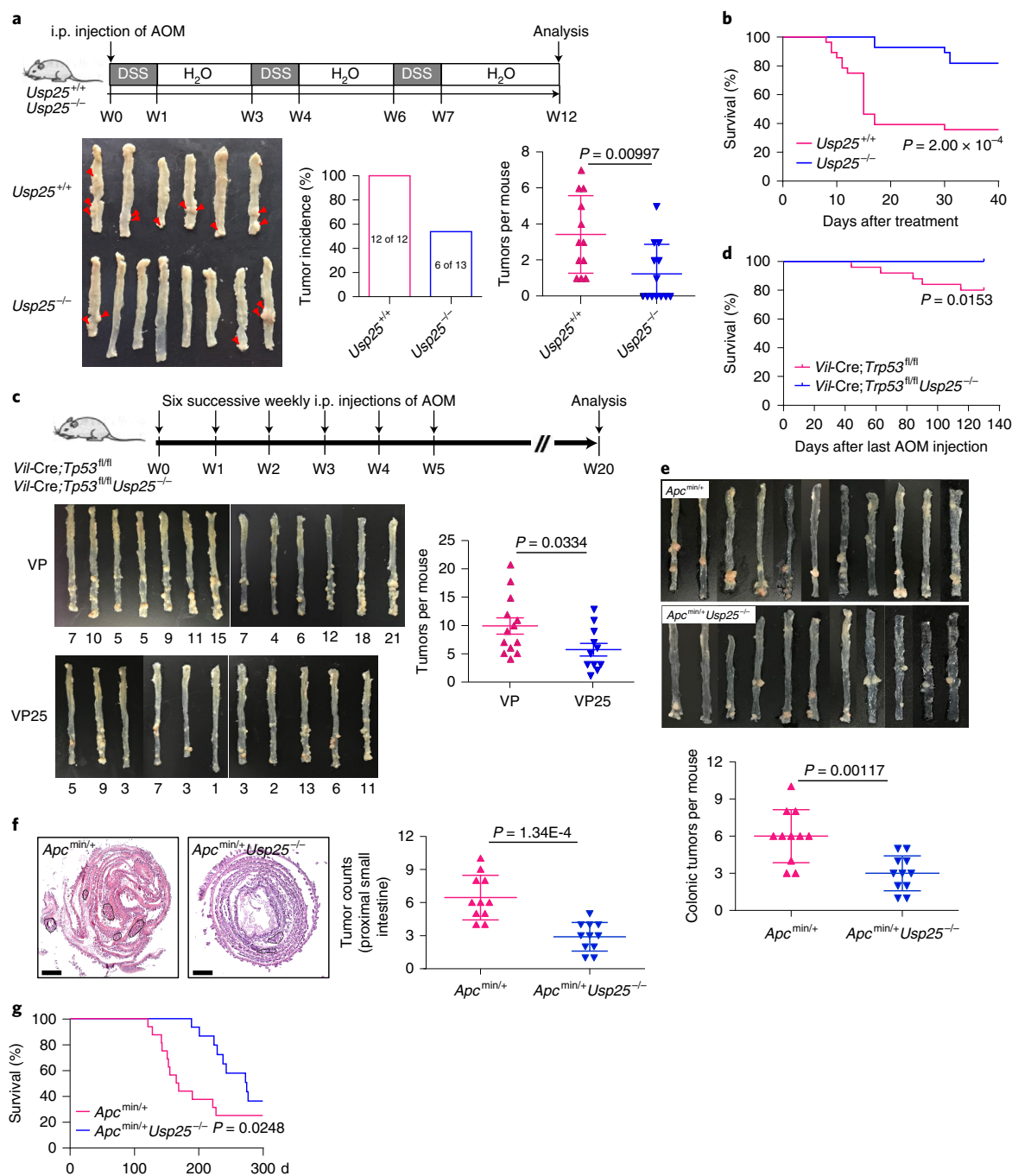


Fig. 4 | USP25 deficiency inhibits tumorigenesis in the colon. **a**, A scheme of AOM/DSS colon cancer model (top). Images of (lower left), tumor incidence (lower middle) and tumor counts (lower right) in colons from female *Usp25*^{+/+} ($n = 12$) and *Usp25*^{-/-} ($n = 13$) mice that were induced with colon cancer with the AOM/DSS protocol. i.p., intraperitoneal. **b**, Survival of male *Usp25*^{+/+} ($n = 28$) and *Usp25*^{-/-} ($n = 28$) mice that were induced with colon cancer as in **a**. **c**, A scheme of induction of colon tumors with the AOM/*Vil-Cre;Trp53*^{fl/fl} model (upper). Images (lower left) and tumor counts (lower right) in colons of *Vil-Cre;Trp53*^{fl/fl} ($n = 13$) and *Vil-Cre;Trp53*^{fl/fl}*Usp25*^{-/-} ($n = 11$) mice that were injected weekly with AOM (10 mg per kg body weight, i.p.) for 6 weeks successively and killed at the 20th week after initial AOM injection. **d**, Survival of *Vil-Cre;Trp53*^{fl/fl} ($n = 25$) and *Vil-Cre;Trp53*^{fl/fl}*Usp25*^{-/-} ($n = 27$) mice that were induced with colon cancer as in **b**. **e**, Images and statistical analysis of tumor counts in the colons of 5-month-old *Apc*^{Min/+} ($n = 11$) and *Apc*^{Min/+}*Usp25*^{-/-} ($n = 11$) mice. **f**, H&E staining and statistical analysis of tumor counts in intestinal sections from **e**. **g**, Survival of *Apc*^{Min/+} ($n = 19$) and *Apc*^{Min/+}*Usp25*^{-/-} ($n = 15$) mice. Statistical analyses were performed with two-tailed Student's *t*-test (**a,c,e,f**) or log-rank analysis (**b,d,g**). Scale bars, 1 mm (**f**). Data are combined from two (**a**), three (**c**) or four (**b,e,f**) independent experiments (mean \pm s.d. in **a,c,e,f**). Numerical source data for the experiments in this figure can be found in Source Data Fig. 4.

Usp25^{+/+} or *Usp25*^{-/-} mice (Extended Data Fig. 6e,f), indicating low toxicity of AZ1 through oral injection. In addition, AZ1 treatment potentiated *C. rodentium*-induced expression of proinflammatory cytokines and chemokines, whereas it inhibited Wnt3a-induced

expression of downstream genes in *Usp25*^{+/+} but not *Usp25*^{-/-} colon organoids (Extended Data Fig. 7a,b), suggesting selective inhibition of AZ1 on USP25 downstream of bacterial infections or Wnt stimulation. The replication of *C. rodentium*, ST or *E. coli* DH5 α

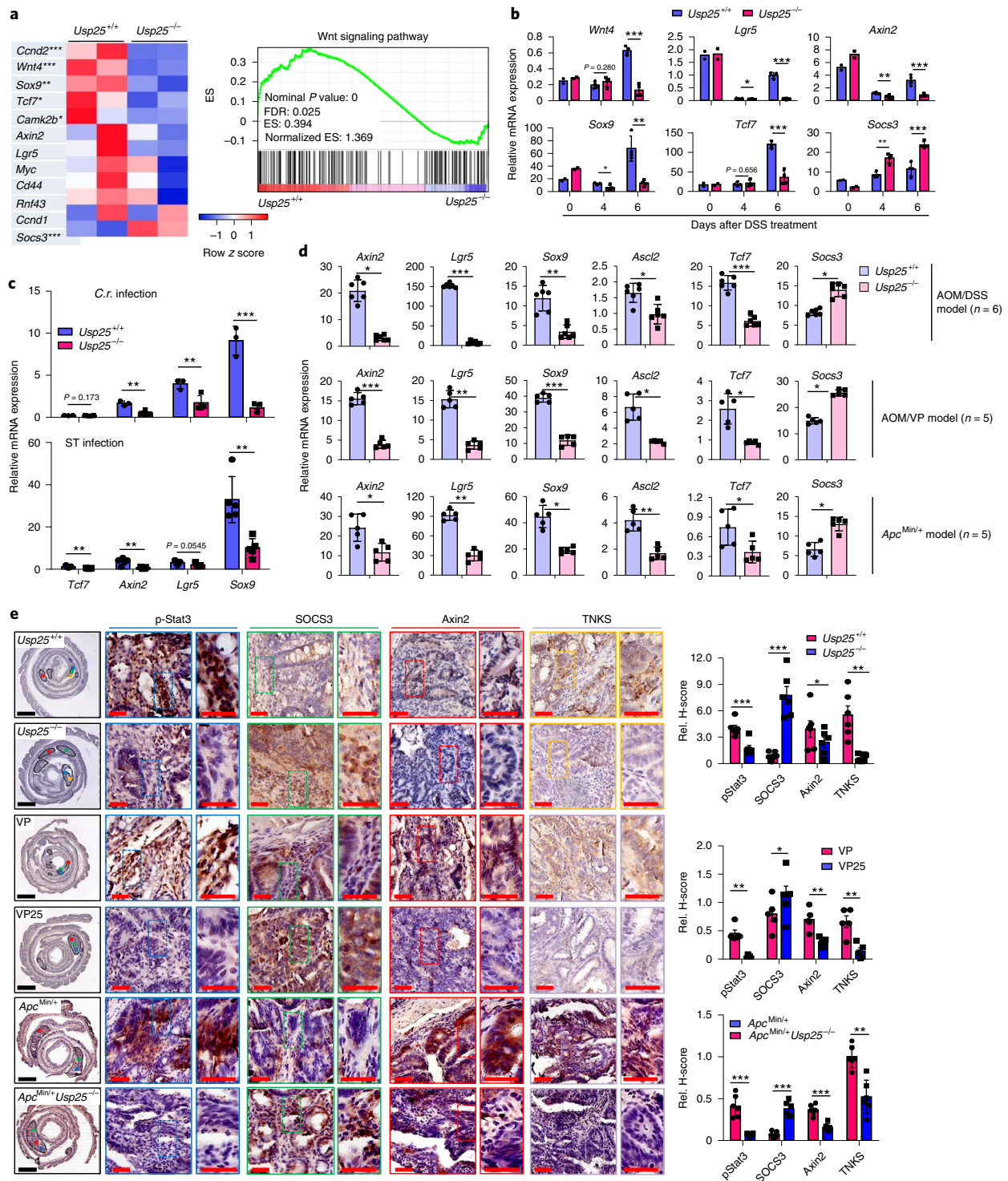


Fig. 5 | USP25 deficiency impairs Wnt signaling and upregulates Socs3. **a**, Heat map of selected Wnt signaling pathway genes and *Socs3* and GSEA analysis of Wnt signaling pathway from the transcriptome profiles of colon tissues from *Usp25*^{+/+} (*n* = 2) and *Usp25*^{-/-} (*n* = 2) mice that were given 2.5% DSS in drinking water for 5 d, followed by normal drinking water for another 2 d. **b**, qRT-PCR analysis of *Wnt4*, *Lgr5*, *Sox9*, *Axin2*, *Ccnd1* and *Socs3* in colon tissues of *Usp25*^{+/+} (*n* = 2, 4 and 4 at day 0, 4 and 6, respectively) and *Usp25*^{-/-} (*n* = 2, 4 and 4 at day 0, 4 and 6, respectively) mice that were given 2.5% DSS in drinking water for 4 or 6 d. **c**, qRT-PCR analysis of *Tcf7*, *Axin2*, *Lgr5* and *Sox9* in colons from *Usp25*^{+/+} (*n* = 3) or *Usp25*^{-/-} (*n* = 4) mice that were infected by *C. rodentium* (1×10^9 c.f.u.) for 14 d (upper) and qRT-PCR analysis of *Tcf7*, *Axin2*, *Lgr5* and *Sox9* in colons from *Usp25*^{+/+} (*n* = 5) or *Usp25*^{-/-} (*n* = 5) mice that were infected by ST (5×10^6 c.f.u.) for 6 d. **d**, qRT-PCR analysis of Wnt signaling pathway genes and *Socs3* in colon tumors from the AOM/DSS (top graphs, *Usp25*^{+/+}, *n* = 6 mice; *Usp25*^{-/-}, *n* = 6 mice), AOM/VP (middle graphs, *Usp25*^{+/+}, *n* = 5 mice; *Usp25*^{-/-}, *n* = 5 mice) and *Apc*^{Min/+} (bottom graphs, *Usp25*^{+/+}, *n* = 5 mice; *Usp25*^{-/-}, *n* = 5 mice) mouse colon cancer models. **e**, IHC images and intensity quantification of Axin2, SOCS3, p-Stat3 and TNKS proteins in USP25-sufficient or deficient colon tumors from AOM/DSS, AOM/*Vil-Cre*;*Trp53*^{fl/fl} and *Apc*^{Min/+} models. **P* < 0.05; ***P* < 0.01; ****P* < 0.001 (two-way ANOVA in **b** or two-tailed Student's *t*-test in **c–e**). Red and black scale bars, 50 μ m and 1 mm, respectively (**e**). Data are representative of two (**b–e**) independent experiments (mean \pm s.d. in **b–e**). Numerical source data for the experiments in this figure can be found in Source Data Fig. 5.

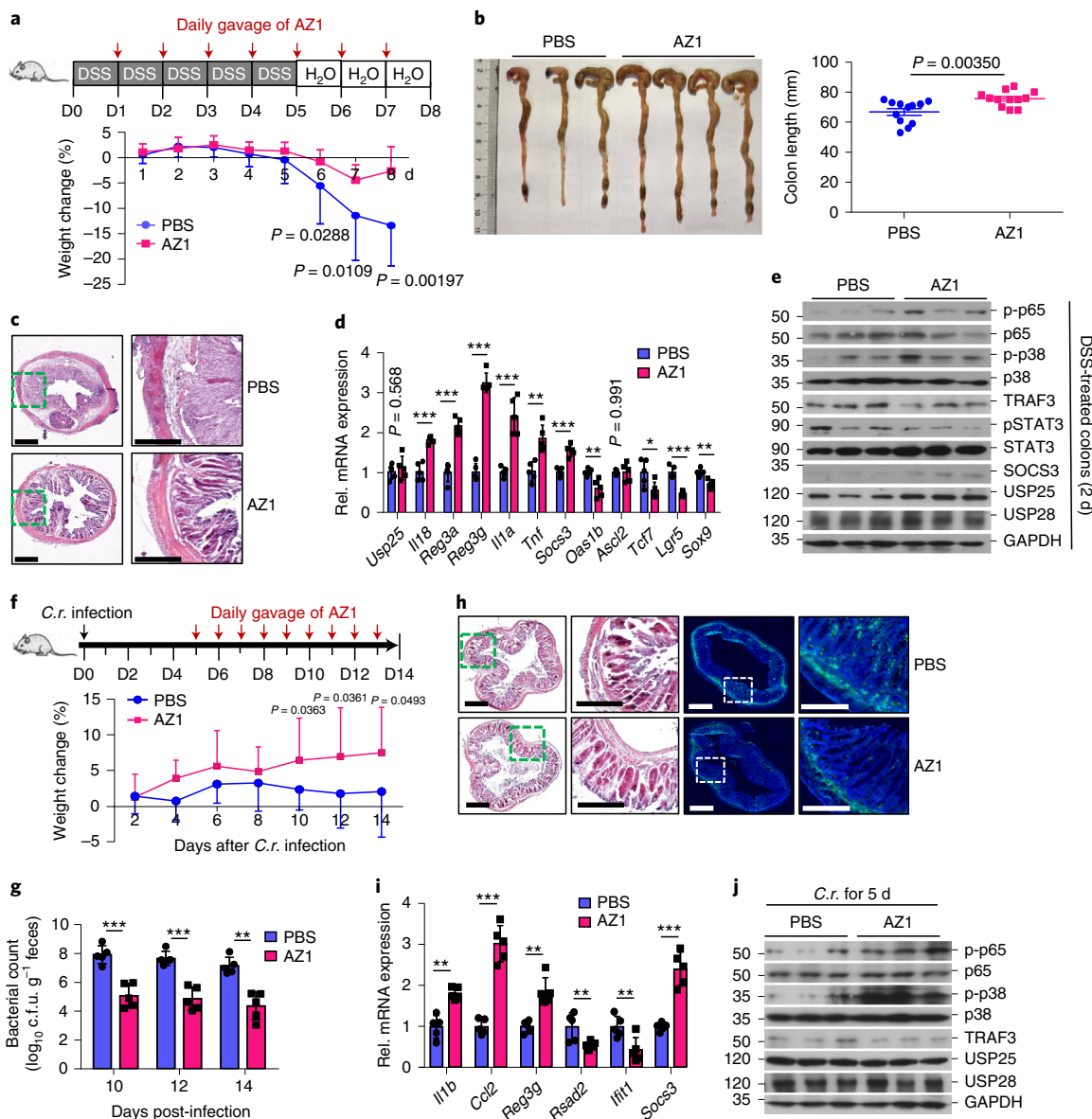


Fig. 6 | Targeting USP25 impairs DSS-induced colitis and restricts bacterial infections. **a**, A scheme of DSS and AZ1 treatment (top) and body weight change (bottom) of WT mice that were induced with colitis by a protocol of 5 d of 2.5% DSS and 3 d of water and administered by gavage with PBS ($n=12$) or AZ1 (40 mg per kg body weight) ($n=12$) for 7 d successively. **b,c**, Morphological change of representative colons and colon lengths (**b**) ($n=12$ mice for PBS and AZ1 groups) and representative images of H&E-stained colon sections (**c**) from mice treated as in **a**. **d**, qRT-PCR analysis of indicated genes in colons of mice treated as in **a** ($n=5$ mice for PBS and AZ1 groups). **e**, Immunoblot analysis of indicated proteins in colon tissues from mice that were treated with 2.5% DSS in the presence of PBS or AZ1 gavage for 2 d ($n=3$ mice for PBS and AZ1 groups). **f**, A scheme of *C. rodentium* infection and AZ1 treatment (top) and body weight change (bottom) of WT mice (PBS, $n=9$; AZ1, $n=10$) that were infected with *C. rodentium*, followed by daily injection of AZ1 by gavage (40 mg per kg) at 5–13 d after infection with *C. rodentium*. **g**, Bacterial counts in fecal homogenates of mice treated as in **e** at 10, 12 and 14 d after infection with *C. rodentium* ($n=5$ mice for PBS and AZ1 groups). **h**, Representative images of H&E-stained colon sections (left two columns) and representative immunofluorescent staining images (anti-*C. rodentium*) of colon sections from mice treated as in **f**. **i**, qRT-PCR analysis of indicated genes in colon tissues from mice treated as in **f** ($n=5$ mice for PBS and AZ1 groups). **j**, Immunoblot analysis of indicated proteins in colon tissues from mice that were infected with *C. rodentium* in the presence or absence of AZ1 gavage for 5 d ($n=3$ mice for PBS and AZ1 groups). * $P < 0.05$; ** $P < 0.01$; *** $P < 0.001$ (two-tailed Student's *t*-test in **a,b,d,f,g,i**). Scale bars, 0.4 mm (**c,h**). Data are combined of three (**a,b**) or two (**f**) independent experiments or representative of three (**c-e**) or two (**f-h**) independent experiments (mean \pm s.d. in **a,b,d,f,g,i**). Uncropped immunoblot images and numerical source data for experiments in this figure are in Source Data Fig. 6.

was not affected by AZ1 in LB medium cultures (Extended Data Fig. 7c). Moreover, the composition and diversity of gut microbiota in feces were similar between PBS- and AZ1-treated groups (Extended Data Fig. 7d,e and Supplementary Table 4), indicating that AZ1 neither exhibits direct toxicity to bacteria nor affects the microbiota in the gut.

We next investigated the effects of AZ1 on DSS-induced colitis and found that AZ1 gavage protected from weight loss and diarrhea and impaired colon shortening and potentiated the expression of proinflammatory cytokines and antibacterial peptides in colons of *Usp25*^{-/-} mice compared to control counterparts (Fig. 6a–d). In addition, levels of p-p65, p-p38 and SOCS3 were

potentiated and levels of TRAF3 and pSTAT3 were decreased in colon tissues from AZ1-treated mice compared to PBS-treated mice (Fig. 6e). In contrast, AZ1 gavage did not alleviate DSS-induced colitis in *Usp25*^{-/-} mice or the spontaneous colitis of *Il10*^{-/-} mice (Extended Data Fig. 7f–k). In addition, gavage of AZ1 maintained weight gain and reduced the bacteria count in feces compared to the PBS group after *C. rodentium* infection (Fig. 6f,g). Consistently with these data, inflammation and bacterial replication in the colon were impaired, expression of proinflammatory cytokines and anti-bacterial peptides was potentiated, levels of p-p65 and p-p38 were increased and levels of TRAF3 were decreased in colons of mice with AZ1 gavage compared to controls (Fig. 6h–j). These data collectively suggest that inhibition of USP25 effectively alleviates colitis and restricts bacterial infections in the GI tract.

Inhibition of USP25 impairs colon cancer development. We next determined whether targeting USP25 would be of benefit for inhibition of colon cancer. In the AOM/DSS model, AZ1 treatment significantly reduced tumor numbers in colons compared to the PBS group (Fig. 7a,b). Expression of Wnt-related genes and levels of pSTAT3 were decreased and levels of SOCS3 were increased in tumors of the AZ1-treated group compared to the control group (Fig. 7c–e). In the VP model, AZ1 treatment significantly inhibited tumorigenesis in the colon and prolonged the survival of VP mice (Fig. 7f,g). Similarly, levels of Wnt-related genes and pSTAT3 were significantly inhibited and levels of SOCS3 were potentiated in tumors of the AZ1-treated group compared to the control group (Fig. 7h–k). In contrast, AZ1 treatment had minimal effect on tumorigenesis in the USP25-deficient background (Extended Data Fig. 8a,b). These findings support the notion that targeting USP25 inhibits colon tumorigenesis.

Discussion

We have previously demonstrated an essential role of USP25 in restricting TLR-triggered induction of proinflammatory cytokines by deubiquitinating and stabilizing TRAF3 (refs. 22,23). Here we show that knockout or pharmacological inhibition of USP25 potentiates immune responses against bacterial infections and alleviates inflammation and tumorigenesis in the GI tract (Extended Data Fig. 8c). TLRs are highly expressed in gut ECs, goblet cells and Paneth cells, which are essential for gut microbial communities and inflammatory bowel diseases^{37–40}. The numbers of goblet cells and Paneth cells are increased in the intestine of *Usp25*^{-/-} mice compared to *Usp25*^{+/+} mice. Therefore, increased numbers of secretory cells and enhanced TLR signaling in secretory cells and ECs from *Usp25*^{-/-} intestines may be responsible for protection against DSS-induced colitis and bacterial infections. In this context, we found that USP25 in nonhematopoietic cells played essential roles in DSS-induced colitis.

We found that depletion of bacteria leads to loss of protection against DSS-induced colitis in *Usp25*^{-/-} mice, which highlights a primary regulatory role of USP25 in commensal bacteria-induced signaling during chemically induced colitis. Although the exact

mechanisms are not fully understood, it might be due to a systemic alteration of cytokine and chemokine production in *Usp25*^{-/-} colons versus *Usp25*^{+/+} colons after DSS challenge. For example, *Usp25*^{-/-} colons or colon organoids upregulated *Il1b* expression after DSS treatment or TLR engagement and mice deficient in IL-1β or IL-1R exhibit hyper-sensitivity to DSS-induced colitis or bacterial infections^{41,42}. *Il18* polymorphisms known to reduce *Il18* mRNA and protein levels are positively associated with susceptibility to Crohn's disease and IL-18 or IL-18R1 deficiency increases frequencies of colonic CD4⁺IL-17A⁺ and CD4⁺IFN-γ⁺ T cells^{43,44}. Consistently, we found that IL-18 was upregulated by USP25 deficiency in the DSS-induced colitis model, which was associated with decreased frequencies and numbers of CD4⁺IL-17A⁺ and CD4⁺IFN-γ⁺ T cells after DSS treatment. CCL2 and CXCL1 are potent attractants for neutrophils, which are higher in *Usp25*^{-/-} colons than in *Usp25*^{+/+} colons after DSS treatment. However, we observed fewer neutrophils infiltrated in the lamina propria of *Usp25*^{-/-} colons. Neutrophils are of short half-life (~5–10h) and undergo apoptosis after degranulation and activation of reactive oxygen species upon phagocytosis and lysis of bacteria⁴⁵. Apoptotic neutrophils are engulfed by macrophages, which is essential for wound healing^{46,47}. In this context, we observed increased percentages and numbers of CD11b⁺F4/80⁺ macrophages in the lamina propria of *Usp25*^{-/-} colons compared to *Usp25*^{+/+} colons, which might contribute to more efficient epithelial repair and clearance of CD11b⁺Ly6G⁺ neutrophils. Although USP25 deficiency potentiates expression of proinflammatory cytokines in DSS-induced acute colitis, levels of proinflammatory cytokines are comparable between USP25-sufficient and -deficient tumors in chronic inflammatory colon cancer models, indicating that USP25 is involved in regulation of early and acute phases of inflammation and has a limited regulatory role in late and chronic phases. Consistently with this notion, inhibition of USP25 by AZ1 in *Il10*^{-/-} mice did not affect development of spontaneous chronic colitis.

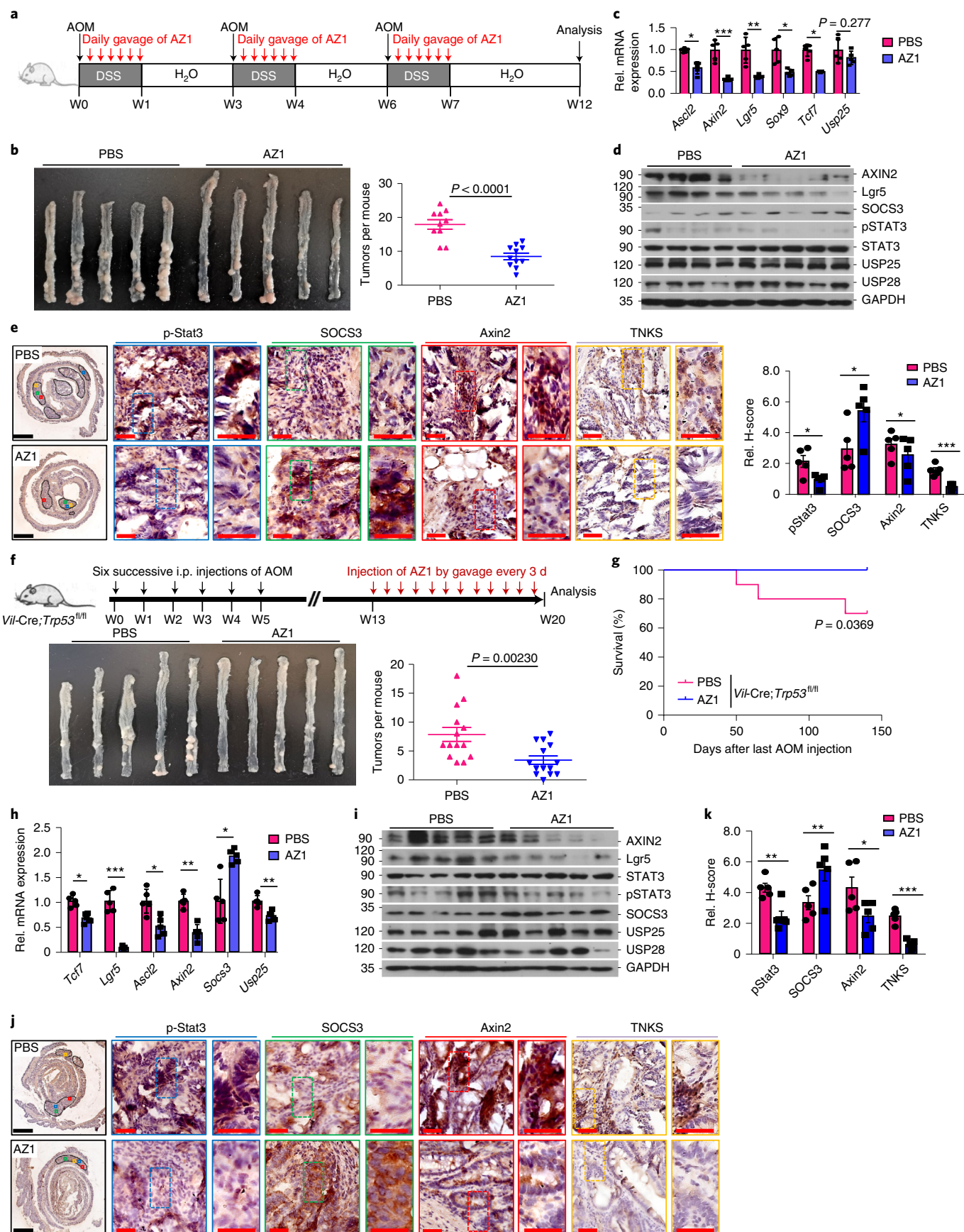
Wnt signaling is required for epithelium repair after DSS treatment⁴⁸. Although Wnt signaling is impaired by USP25 deficiency, *Usp25*^{-/-} mice maintain the integrity of colon epithelium compared to *Usp25*^{+/+} mice after DSS challenge. A possible explanation for this is that elevated levels of proinflammatory cytokines facilitate epithelium repair with a requirement of fewer Wnt-β-catenin signals. In this context, it has been shown that epithelial TNF-α-TNF receptor signaling facilitates Wnt-β-catenin signaling in mucosal repair in IBD⁴⁹. In addition, increased levels of SOCS3 and decreased levels of pSTAT3 are observed in USP25-deficient colon tumors or inflamed colon tissues compared to USP25-sufficient counterparts, consistently with previous reports that SOCS3 is a major regulator of inflammation by inhibiting STAT3 phosphorylation^{34,35,50,51}.

Accumulating evidence suggests critical roles of gut bacteria in CRC development by directly activating protumor factors or indirectly providing toxic factors⁵². Our study has revealed crosstalk between bacterial infections and protumor factors that are connected by USP25. USP25 is upregulated in colon tissues (most likely in the

Fig. 7 | USP25 is a therapeutic target for colon cancer. **a**, A scheme of AZ1 treatment during the induction of AOM/DSS colon cancer. **b**, Tumor counts of colons from WT mice that were induced with colon cancer with the AOM/DSS protocol and injected daily with AZ1 (20 mg per kg) ($n=11$) or PBS ($n=10$) by gavage during three rounds of DSS treatment. **c–e**, qRT-PCR (**c**) ($n=5$ mice for PBS and AZ1 groups), immunoblot (**d**) (PBS, $n=4$ mice; AZ1, $n=5$ mice) and representative images of IHC and quantification analysis (**e**) ($n=5$ mice for PBS and AZ1 groups) of indicated genes or proteins in colon tumors from mice treated as in **a**, **f**. A scheme of AZ1 treatment during induction of AOM/*Vil-Cre*;*Trp53*^{fl/fl} model (top). Images (bottom left) and tumor counts (bottom right) of colons from *Vil-Cre*;*Trp53*^{fl/fl} mice that were injected weekly with AOM (10 mg per kg) for 6 weeks successively, followed by injection of AZ1 (20 mg per kg) ($n=14$) or PBS ($n=14$) by gavage every 3 d from 13–20 weeks after initial AOM injection (bottom). **g**, Survival of *Vil-Cre*;*Trp53*^{fl/fl} (PBS, $n=10$; AZ1, $n=13$) mice treated as in **f**. **h–j**, qRT-PCR (**h**), immunoblot (**i**) and representative images of IHC and quantification analysis (**j**) of indicated proteins or genes in colon tumor tissues from mice treated as in **f** ($n=5$ mice for PBS and AZ1 groups). * $P < 0.05$; ** $P < 0.01$; *** $P < 0.001$ (two-tailed Student's *t*-test in **b,c,e,h,k** or log-rank analysis in **g**). Red and black scale bars, 50 μm and 1 mm (**e,j**), respectively. Data are combined from two (**b,g**) or three (**f**) independent experiments or representative of two (**c–e,h–k**) independent experiments (mean ± s.d. in **b,c,e,f,h,k**). Uncropped immunoblot images and numerical source data for the experiments in this figure are in Source Data Fig. 7.

epithelial layer cells and possibly in LPMCs) by bacterial infections or DSS treatment, which has at least three functions. (1) It modulates the TLR–TRAF3–p65/p38 signaling axis and downstream

cytokine expression, which leads to impaired antibacterial immune responses and aggravated inflammation in the colon. (2) It inhibits SOCS3 expression in a manner dependent on gut bacteria, which



leads to potentiated phosphorylation of STAT3. (3) It facilitates Wnt signaling in colon tissues during bacterial infection or colitis development. Together, available data suggest a gut bacterial infection- or colonization-mediated connection between USP25-mediated regulation of colonic inflammation and tumorigenesis.

AZ1 is a dual inhibitor for USP25 and USP28 (ref. 36). Notably, AZ1 significantly inhibits *C. rodentium*- or Wnt-induced expression of downstream genes in *Usp25^{+/+}* but not in *Usp25^{-/-}* colon organoids and attenuates DSS-induced colitis and tumorigenesis in the colons of *Usp25^{+/+}* mice but not *Usp25^{-/-}* mice. In addition, our transcriptome sequencing data and others' single-cell RNA-seq data suggest that expression levels of *Usp25* in gut tissue are much higher (3–4-fold) than those of *Usp28* and that DSS treatment upregulates *Usp25* but not *Usp28* mRNA levels^{25,26}. It is thus likely that USP25, but not USP28, is the primary target of AZ1 or that USP25 plays a major role (compared to USP28) in these pathways or models. However, we could not rule out the possibility that USP28 functions downstream of USP25 in related pathways or models. Further investigations with USP25-specific inhibitors are required to fully address this point. Nonetheless, our preclinical data using a pharmacological inhibitor of USP25 provides an effective therapy for inflammation and cancers in the GI tract.

Methods

Mice. *Usp25^{-/-}* mice were described previously²³. B6.SJL (002014), *Trp53^{fl/fl}* (008462) and *Ifnar1^{-/-}* (032045) mice were purchased from Jackson Laboratory. WT C57BL/6 mice, *Villin-Cre* (T000142) and *Apc^{Min/+}* (T001457) mice were from GemPharmatech. *Usp25^{+/+}* and *Usp25^{-/-}* (from *Usp25^{+/+}* breeders) or *Ifnar1^{-/-}* and *Ifnar1^{-/-}Usp25^{-/-}* (from *Ifnar1^{-/-}Usp25^{+/+}* breeders) littermates were used throughout the study. *Villin-Cre;Trp53^{fl/fl}* and *Villin-Cre;Trp53^{fl/fl}Usp25^{-/-}* mice were bred independently. Male *Apc^{Min/+}* and *Apc^{Min/+}Usp25^{-/-}* mice were bred with female *Usp25^{+/+}* and *Usp25^{-/-}* littermates, respectively. No statistical methods were used to predetermine sample size. For all experiments presented in this study, age-matched (8–10 weeks old) and sex-matched (both male and female) mice were used and sample sizes were large enough to determine statistically significant effects. The control and experimental groups of mice were co-housed and randomly allocated to different treatments. All mice were housed in a specific-pathogen-free (SPF) animal facility at Wuhan University with a 12-h dark/12-h light cycle and fed with standard food and water. *Il10^{-/-}* mice (002251, C57BL/6J) background, male, 8-week-old, SPF) were derived from Jackson Laboratory by Cavens Laboratory Animal Co. Immediately after arrival, these mice were housed in conventional conditions (open cages). At 12 weeks old, these mice were injected with PBS or AZ1 (40 mg per kg body weight) by gavage every 3 d for 8 weeks.

Human material. Colorectal tumor samples were collected between November 2016 and November 2017 at the Department of Pathology of Zhongnan Hospital of Wuhan University (Supplementary Table 3). Tumor tissues were fixed with 4% paraformaldehyde and embedded in paraffin blocks. The tissue array was prepared as previously described²⁴ and subjected to IHC or fluorescence in situ hybridization (FISH) analysis.

DSS-induced colitis and colon cancer models. For the DSS-induced colitis model, mice were administered the indicated dosage of DSS dissolved in sterile water for 5 d, followed by regular water for 1–3 d. For the AOM/DSS colorectal tumor model, co-housed experimental mice were injected i.p. with 10 mg per kg azoxymethane (AOM; Sigma), followed by treatment of 2.5% DSS drinking water for 7 d and regular water for 14 d. This cycle was repeated three times and mice were killed 3 weeks after the end of the last DSS cycle or immediately after the last DSS cycle. For the *Villin-Cre;Trp53^{fl/fl}* colon cancer model, 8-week-old mice were injected i.p. with AOM (10 mg per kg) once per week for 6 weeks successively. At the 18–20th week after the initial AOM injection, colons were collected, washed to remove feces with cold PBS and slit open longitudinally to count tumors or monitored for survival for 20 weeks after the last injection of AOM. For the *Apc^{Min/+}* colon cancer model, mice were fed with normal food and water for 5 months. For *F. nucleatum* infection-induced colon cancer, *Apc^{Min/+}* and *Apc^{Min/+}Usp25^{-/-}* mice (6 weeks old) were orally injected with *F. nucleatum* (1×10^8 c.f.u. per mouse) for 8 weeks successively. Colons and intestines were collected, washed and slit open longitudinally for various analyses.

RNA-seq and 16S rRNA-seq. Colons were flushed with PBS to clear feces and slit open longitudinally. Distal colon tissues (0.5 cm in length, about 0.5 cm away from the anus) were washed in PBS and homogenized in 2 ml of TRIzol (Invitrogen). Total RNAs were prepared and the quality of RNAs was determined by agarose gel electrophoresis and spectrophotometer analysis. Poly(A) mRNA

was subsequently purified from 10 µg total RNA using NEBNext Oligo d(T)₂₅ Magnetic Beads Isolation Module. First-strand complementary DNA was synthesized with NEBNext RNA First-Strand Synthesis Module. NEBNext Ultra II Non-Directional RNA Second Strand Synthesis Module was used for the synthesis of the complementary strand of first-strand cDNA. The resulting double-stranded DNA was purified and Vazyme TruePrep DNA Library Prep kit V2 was used to prepare libraries followed by sequencing on an Illumina HiSeq X Ten platform with 100-bp paired-end reads strategy (Novogene). Quality control of mRNA-seq data was performed by using Fatsqc and low-quality bases were trimmed by Cutadapt. All RNA-seq data were mapped to the mouse genome (mm9) by TopHat (v.2.1.1) and allowed a maximum of two mismatches per read. Gene expression level was calculated by Cufflinks with default parameters and normalized by FPKM.

Mice were treated with or without AZ1 gavage (40 mg per kg body weight) and simultaneously fed with normal water or 2.5% DSS for 6 d. Collected colons were split open and feces were collected and frozen into liquid nitrogen until analysis. Total genome DNA from samples was extracted using the CTAB/SDS method. DNA concentration and purity were monitored on 1% agarose gels. According to the concentration, DNA was diluted to 1 ng µl⁻¹ using sterile water. 16S rRNA genes of distinct regions (16S V4/16S V3/16S V3-V4/16S V4-V5) were amplified using specific primers (for example, 16S V4:515F-806R) with the barcode. All PCR reactions were carried out with 15 µl of Phusion High-Fidelity PCR Master Mix (New England Biolabs); 0.2 µM of forward and reverse primers and about 10 ng of template DNA. PCR products were mixed in equidensity ratios and purified with Qiagen Gel Extraction kit (Qiagen). Sequencing libraries were generated using TruSeq DNA PCR-Free Sample Preparation kit (Illumina) following manufacturer's recommendations and index codes were added. Library quality was assessed on the Qubit@ 2.0 Fluorometer (Thermo Fisher Scientific) and Agilent Bioanalyzer 2100 system. The library was sequenced on an Illumina NovaSeq platform and 250-bp paired-end reads were generated.

Bone marrow transfer and preparation of lamina propria leukocytes. The experiments were performed as previously described⁵⁵. Recipient mice were irradiated with 10 Gy and isolated bone marrow cells were immediately injected through tail vein (10^6 cells per mouse). Colon pieces were incubated with RPMI 1640 supplemented with 10% FBS, 5 mM EDTA, 1 mM DTT and 50 µg ml⁻¹ gentamicin and shaken at 220 r.p.m. at 37 °C for 30 min. Tissues were then incubated with RPMI 1640 containing 10% FBS, 50 U ml⁻¹ DNase I and 0.5 mg ml⁻¹ collagenase type IV for 30 min at 37 °C with shaking at 220 r.p.m. Liberated cells were collected by passage through a nylon mesh. Isolated cells from the collagenase-treated fractions were separated on a 40/80% discontinuous Percoll gradient.

Bacterial strains, growth conditions and infections. *C. rodentium* (ICC169) and ST were described previously⁵⁶ and kindly provided by S. Li (Huazhong Agricultural University). *F. nucleatum* was cultured and the c.f.u. of *F. nucleatum* was determined as previously described³². Mice were injected by gavage with approximately 1×10^7 c.f.u. of ST or 1×10^9 c.f.u. of *C. rodentium* suspended in 200 µl of sterile PBS. The weight and survival of mice were monitored daily. At indicated time points after infection, mice were killed and the colon and spleen were removed for analysis. For analysis of fecal bacteria count, fresh feces were collected and dissolved in sterile PBS, which was serially diluted and placed on conditional LB agar plates. The bacterial colonies were counted after incubation at 37 °C for 24 h. For analysis of inflammation and bacterial replication in the colons, the colons were fixed in 4% paraformaldehyde and embedded in paraffin followed by H&E staining or frozen in Tissue-Tek O.C.T. compound (Thermo Fisher Scientific, 4583) for immunofluorescent staining, respectively.

Fluorescence in situ hybridization. The sections were baked at 90 °C for 1 h and deparaffinized by twice immersing in xylenes for 10 min, followed by immersing in 100% (v/v, 5 min), 85% (3 min) and 75% (3 min) ethanol. Sections were immersed in HCl (0.2 M) for 15 min at room temperature followed by two washes with PBS. Proteinase K (50 µg ml⁻¹, 500 µl) was added to cover the slices (37 °C for 15 min) and removed by three washes with PBS. The sections were dehydrated in 70%, 85% and 100% (v/v) ethanol (3 min and 500 µl each) and dried in a fume hood at room temperature. The probes (2 µg) diluted in hybridizing buffer (200 µl, 0.7 M NaCl, 0.1 M Tris (pH 8.0), 0.1% sodium dodecyl sulfate, 10 mM EDTA) were applied to the surface of the slices that were put into a moisture-sealed slide incubation chamber. The samples on slices were hybridized by denature for 8 min at 85 °C and subsequent annealing for overnight at 37 °C. DAPI-antifade solution was added on the sections that were covered by a cover slide and incubated for 10 min. The covered slides were imaged with a fluorescence microscope and FISH spots were counted. Probes were labeled by Cy3 and the sequence for *F. nucleatum* FISH assay was 5'-CTTGATGTTCCGGYTACCTC-3' (FUS664, Exon Biotechnology).

Colon organoid culture. Colon tissues were vigorously shaken in 2 mM EDTA for 1 h at 4 °C, followed by removing the EDTA solution. Subsequently loosened crypts were prepared by pipetting the solution up and down with 15 ml of PBS through a 10-ml pipette for 8–10 times followed by 1 min rest. The supernatants containing the crypt suspension were transferred into a new 50-ml centrifuge tube and precipitants were re-suspended with 15 ml of PBS and pipetted up and down

for repeated collection of crypts. FBS was added to the crypt suspensions at a final concentration of 10%. Supernatants containing crypts were centrifuged at 300g for 5 min. Pelleted crypts were re-suspended in 2 ml of conditional medium with growth factors (CMGF advanced DMEM/F12) and collected by centrifugation at 130g for 5 min at 4 °C. Finally crypts were suspended in Matrigel (Corning) and placed in the center well of a 24-well plate (40 µl per well). After the Matrigel had solidified (15 min at 37 °C), crypts were cultured in culture medium (200 ng ml⁻¹ R-spondin, 10 ng ml⁻¹ Noggin, 1 mM *N*-acetyl cysteine, 10 mM nicotinamide, 0.5 µM A83-01, 3 µM SB202190, 50 ng ml⁻¹ EGF, 1 × B27 and 1 × N2) at 37 °C with 5% CO₂. Culture medium was refreshed every 2–3 d. Organoids were treated by Wnt3a or LPS or infected with *C. rodentium* or ST SL1344 at day 6–7 after culture.

H&E staining. Colon tissues from mice with DSS-induced colitis or colonic tumors were fixed in 4% paraformaldehyde and embedded in paraffin blocks. The paraffin blocks were sectioned (5 µm) for H&E staining (Beyotime Biotech) followed by cover-slipping. Images were acquired with an Aperio VERSA 8 (Leica) multifunctional scanner. Pathogenic scores of inflamed colons were evaluated by combining disease activity index (DAI) score and histopathological score. DAI score was assessed for each animal as a cumulative score for severity of colitis, according to stool consistency (score: 0, normal; 1, soft and shaped; 2, loose stools; 3, diarrhea), rectal bleeding (score: 0, normal; 1 and 2, bloody stool; 3, gross bleeding) and body weight loss (score: 0, none; 1, 1%–5%; 2, 5%–10%; 3, 10%–15%; 4, >15%). Histopathological changes were analyzed as a cumulative score, on the basis of epithelial damage (0, normal morphology; 1, loss of goblet cells; 2, loss of goblet cells in large areas; 3, loss of crypts; 4, loss of crypts in large areas) and inflammatory cell infiltration (0, no infiltration; 1, infiltration around crypt bases; 2, infiltration spreading to muscularis mucosa; 3, extensive infiltration in the muscularis mucosa with abundant edema; 4, infiltration spreading to submucosa).

Flow cytometry analysis. Single-cell suspensions were re-suspended in FACS buffer (PBS, 1% BSA) and blocked with anti-mouse CD16/32 antibodies for 10 min before staining with specific antibodies. Antibodies against cell surface markers: anti-CD3-PE (BioLegend, 100308), anti-CD4-FITC (100406), anti-CD8-BV510 (100751), anti-CD11b-FITC (101206), anti-CD11c-PerCP (117328), anti-Gr-1-APC (108411), anti-F4/80-PE (123110), anti-CD19-APC (M10191-11c), anti-GL7-PerCP (144610), anti-FAS-PE (152608), anti-CD62L-APC (104412) and anti-CD44-PE (MH10441-09D). For intracellular cytokine staining, cells were fixed and permeabilized using a fixation and permeabilization solution (eBioScience, 50-112-9060). Antibodies used for intracellular cytokine staining were anti-IL-17A-APC-Cy7 (506939), anti-Foxp3-APC (126408) and anti-IFN-γ-PerCP (505822). Flow cytometry data were acquired on a FACSCelesta flow cytometer and analyzed with FlowJo.

Immunoblot, IHC, ELISA and qRT-PCR assays. These experiments were performed as previously described^{54,57,58}. Primary antibodies used were anti-USP25 (A7975, AbClonal), anti-USP28 (17707-1-AP, Proteintech), anti-pStat3 (9145S, Cell Signaling Technology), anti-p-p65 (3033S), anti-p-p38 (9216S), anti-GAPDH (5174), anti-Stat3 (SC-8019, Santa Cruz Biotechnology), anti-p65 (SC-372), anti-p38 (SC-7149), anti-Igr5 (A12987, AbClonal), anti-Axin2 (A2513) and anti-Socs3 (A0694). Secondary antibodies used were HRP-conjugated goat-anti-mouse or rabbit IgG (Thermo Fisher Scientific, PA1-86717 and SA1-9510). Histological analysis for inflammation, epithelial hyperplasia and tumorigenesis was performed by a board-certified pathologist (Z. Xu). Signals were imaged with an Aperio VERSA 8 (Leica) multifunctional scanner and quantified with the software Image-Pro Plus 6.0. Concentrations of TNF-α and IL-6 in the sera from mice infected with ST or *C. rodentium* were measured by ELISA (LEGENDplex Multi-Analyte Flow Assay kit, BioLegend).

Total RNA was extracted from distal colons of mice after colitis induction, colon tumor tissues or organoids using TRIzol (Invitrogen) and resolved in 200 µl of RNase-free water and mixed with 20 µl of 8 M LiCl buffer followed by centrifugation at 14,000g for 30 min. Precipitants were dissolved in 200 µl of RNase-free water and mixed with 20 µl of 3 M sodium acetate and 400 µl of ethanol followed by centrifugation at 14,000g for 30 min. Precipitants containing RNAs were washed with 75% ethanol, dissolved with 50–100 µl of RNase-free water and quantified for qRT-PCR analysis. The value obtained for each gene was normalized to that of the gene encoding *GAPDH*. Gene-specific primers are listed in Supplementary Table 5.

Generation and HPLC analysis of AZ1. The compound AZ1 was generated by WuXi Apptec with a two-step protocol as follows.

Step 1. K₂CO₃ (977 mg, 7.07 mmol) was added to a solution of compound 1A (711.00 mg, 3.54 mmol) in DMF (6 ml) and the reaction mixture was stirred at 20 °C for 4 h. Then compound 1 (1.0 g, 3.89 mmol) was added and the resultant solution was stirred at 20 °C for 0.5 h. LC-MS analysis showed that the starting material was consumed completely and the desired MS was detected. Ethyl acetate (10 ml) and H₂O (10 ml) was added, the organic layer was washed with brine, dried over Na₂SO₄, filtered and concentrated under reduced pressure to dry to produce compound 2 (1.56 g, crude) as a yellow solid. This was used in the next step directly without purification.

Step 2. The mixture of compound 2 (500 mg, 1.33 mmol) and compound 2A (81 mg, 1.33 mmol) in trimethyl orthoformate (5 ml) was stirred at 25 °C for 3 h. Then the reaction mixture was concentrated under reduced pressure and dissolved in MeOH (5 ml), then NaBH₄ (50 mg, 1.33 mmol) was added at 0 °C and the reaction mixture was stirred at 25 °C for another 1 h. LC-MS analysis showed that the starting material was consumed completely and the desired MS was detected. The reaction was quenched with ice-cold water (0.1 ml) and the mixture was concentrated under reduced pressure, purified by prep-HPLC (Xtimate C18 150 × 25 mm × 5 µm) with water (0.05% ammonia hydroxide (v/v)-CAN) to produce AZ1 (231.88 mg, 0.55 mmol, 41.4% yield, 99.4% purity) as a white solid.

The generated compound (5 mg) was dissolved in MeOH (0.1 ml) and loaded onto a column (XBridge C18, 3.0 × 50 mm, 3.5 µm) on an LC-20 AB instrument (SHIMADZU). The mobile phase consisting of 0.025% NH₃·H₂O in water (v/v) (A) and acetonitrile (B) ran at a rate of 1.2 ml min⁻¹. The gradient was as follows: 70% A and 30% B for 0–3.0 min, 10% A and 90% B for 3.0–3.5 min, 70% A and 30% B for 3.5–4.0 min. Chromatography was detected with a photodiode array at 220 nm, 215 nm and 254 nm.

Treatment with AZ1. AZ1 was dissolved in DMSO (100 mM, 42.2 mg ml⁻¹) and aliquoted for stock until use. For treatment of cells or organoids, the stock was diluted with PBS and added to the culture medium and the final concentration of AZ1 was 5 or 10 µM. For treatment of mice, AZ1 was diluted in 100–200 µl of PBS and injected by gavage according to the body weight of mice (20 or 40 mg per kg body weight).

Study approval. All animal experiments were in accordance with protocols approved by the Institutional Animal Care and Use Committee of Wuhan University. For human samples, protocols in this study were approved by the Institutional Review Committees of Zhongnan Hospital of Wuhan University and the Medical Ethic Committee of the School of Medicine, Wuhan University.

Statistics and reproducibility. Graphs show mean ± s.d. of different mice unless indicated otherwise. ELISA, qRT-PCR and IHC experiments were analyzed by two-tailed Student's *t*-test or two-way ANOVA with Bonferroni test. For animal survival analysis, the Kaplan–Meier method was adopted to generate graphs and survival curves were analyzed by log-rank analysis. RNA-seq data were analyzed by DESeq2 and DAVID 6.8. For correlation analysis, Pearson correlation calculations were performed with Prism 6. Hypergeometric test was performed for KEGG pathway analysis. All analyses above were performed using GraphPad Prism 6 software. A *P* value (or an adjusted *P* value for multiple comparisons) <0.05 was considered statistically significant.

Reproducibility information is provided in the Reporting Summary, including sample size predetermination, randomization, blinding and replication. No statistical method was used to predetermine sample size and no data were excluded from the analyses. The experiments were randomized. The investigators were not blinded to allocation during experiments and outcome assessment.

Reporting Summary. Further information on research design is available in the Nature Research Reporting Summary linked to this article.

Data availability

The RNA-seq and 16S rRNA-seq data that support the findings of this study have been deposited in the Gene Expression Omnibus under accession codes GSE136727 and GSE143003, which can be found in Supplementary Tables 1 and 4, respectively. Hhuman GI cancer data were derived from GEPIA (gepia.cancer-pku.cn). The dataset derived from this resource that supports the findings of this study is available at <http://gepia.cancer-pku.cn/detail.php?gene=USP25###> (cutoff-high, 75%, cutoff-low, 25%; datasets: COAD, READ, STAD). Source data for Figs. 1–7 and Extended Data Fig. 1–8 have been provided as Source Data Figs. 1–7 (numerical source data), Source Data Extended Data Figs. 1–8 (numerical source data), Source Data Figs. 1–3 and 6–7 (uncropped gels) and Source Data Extended Data Figs. 2 and 5 (uncropped gels). All other data supporting the findings of this study are available from the corresponding author upon reasonable request. Source data are provided with this paper.

Received: 8 August 2019; Accepted: 28 May 2020;

Published online: 06 July 2020

References

- Kaser, A., Zeissig, S. & Blumberg, R. S. Inflammatory bowel disease. *Annu. Rev. Immunol.* **28**, 573–621 (2010).
- Somineni, H. K. & Kugathasan, S. The microbiome in patients with inflammatory diseases. *Clin. Gastroenterol. Hepatol.* **17**, 243–255 (2019).
- Jostins, L. et al. Host–microbe interactions have shaped the genetic architecture of inflammatory bowel disease. *Nature* **491**, 119–124 (2012).

4. Hugot, J. P. et al. Association of Nod2 leucine-rich repeat variants with susceptibility to Crohn's disease. *Nature* **411**, 599–603 (2001).
5. Ogura, Y. et al. A frameshift mutation in Nod2 associated with susceptibility to Crohn's disease. *Nature* **411**, 603–606 (2001).
6. Kobayashi, K. S. et al. Nod2-dependent regulation of innate and adaptive immunity in the intestinal tract. *Science* **307**, 731–734 (2005).
7. Maeda, S. et al. Nod2 mutation in Crohn's disease potentiates NF- κ B activity and IL-1 β processing. *Science* **307**, 734–738 (2005).
8. Sokol, H. et al. *Faecalibacterium prausnitzii* is an anti-inflammatory commensal bacterium identified by gut microbiota analysis of Crohn disease patients. *Proc. Natl Acad. Sci. USA* **105**, 16731–16736 (2008).
9. Darfeuille-Michaud, A. et al. Presence of adherent *Escherichia coli* strains in ileal mucosa of patients with Crohn's disease. *Gastroenterology* **115**, 1405–1413 (1998).
10. Ohkusa, T. et al. Induction of experimental ulcerative colitis by *Fusobacterium varium* isolated from colonic mucosa of patients with ulcerative colitis. *Gut* **52**, 79–83 (2003).
11. Bray, F. et al. Global cancer statistics 2018: GLOBOCAN estimates of incidence and mortality worldwide for 36 cancers in 185 countries. *CA: Cancer J. Clin.* **68**, 394–424 (2018).
12. Lasry, A., Zinger, A. & Ben-Neriah, Y. Inflammatory networks underlying colorectal cancer. *Nat. Immunol.* **17**, 230–240 (2016).
13. Dow, L. E. et al. APC restoration promotes cellular differentiation and reestablishes crypt homeostasis in colorectal cancer. *Cell* **161**, 1539–1552 (2015).
14. Greten, F. R. et al. IKK β links inflammation and tumorigenesis in a mouse model of colitis-associated cancer. *Cell* **118**, 285–296 (2004).
15. Schwitalla, S. et al. Loss of p53 in enterocytes generates an inflammatory microenvironment enabling invasion and lymph node metastasis of carcinogen-induced colorectal tumors. *Cancer Cell* **23**, 93–106 (2013).
16. Tauriello, D. V. F. et al. TGF β drives immune evasion in genetically reconstituted colon cancer metastasis. *Nature* **554**, 538–543 (2018).
17. Akira, S., Uematsu, S. & Takeuchi, O. Pathogen recognition and innate immunity. *Cell* **124**, 783–801 (2006).
18. Walsh, D., McCarthy, J., O'Driscoll, C. & Melgar, S. Pattern-recognition receptors—molecular orchestrators of inflammation in inflammatory bowel disease. *Cytokine Growth Factor Rev.* **24**, 91–104 (2013).
19. Rakoff-Nahoum, S., Paglino, J., Eslami-Varzaneh, F., Edberg, S. & Medzhitov, R. Recognition of commensal microflora by Toll-like receptors is required for intestinal homeostasis. *Cell* **118**, 229–241 (2004).
20. Fukata, M. et al. Toll-like receptor-4 is required for intestinal response to epithelial injury and limiting bacterial translocation in a murine model of acute colitis. *Am. J. Physiol. Gastrointest. Liver Physiol.* **288**, G1055–G1065 (2005).
21. Dheer, R. et al. Intestinal epithelial Toll-like receptor 4 signaling affects epithelial function and colonic microbiota and promotes a risk for transmissible colitis. *Infect. Immun.* **84**, 798–810 (2016).
22. Zhong, B. et al. Ubiquitin-specific protease 25 regulates TLR4-dependent innate immune responses through deubiquitination of the adaptor protein TRAF3. *Sci. Signal.* **6**, ra35 (2013).
23. Lin, D. et al. Induction of USP25 by viral infection promotes innate antiviral responses by mediating the stabilization of TRAF3 and TRAF6. *Proc. Natl Acad. Sci. USA* **112**, 11324–11329 (2015).
24. Xu, D. et al. USP25 regulates Wnt signaling by controlling the stability of tankyrases. *Genes Dev.* **31**, 1024–1035 (2017).
25. Kinchen, J. et al. Structural remodeling of the human colonic mesenchyme in inflammatory bowel disease. *Cell* **175**, 372–386 (2018).
26. Tabula Muris, C. et al. Single-cell transcriptomics of 20 mouse organs creates a Tabula Muris. *Nature* **562**, 367–372 (2018).
27. Kitajima, S., Takuma, S. & Morimoto, M. Changes in colonic mucosal permeability in mouse colitis induced with dextran sulfate sodium. *Exp. Anim.* **48**, 137–143 (1999).
28. Yang, Y. et al. *Fusobacterium nucleatum* increases proliferation of colorectal cancer cells and tumor development in mice by activating Toll-like receptor 4 signaling to nuclear factor- κ B, and up-regulating expression of microRNA-21. *Gastroenterology* **152**, 851–866 (2017).
29. Abed, J. et al. Fap2 mediates *Fusobacterium nucleatum* colorectal adenocarcinoma enrichment by binding to tumor-expressed Gal-GalNAc. *Cell Host Microbe* **20**, 215–225 (2016).
30. Rubinstein, M. R. et al. *Fusobacterium nucleatum* promotes colorectal carcinogenesis by modulating E-cadherin/ β -catenin signaling via its FadA adhesin. *Cell Host Microbe* **14**, 195–206 (2013).
31. Kostic, A. D. et al. *Fusobacterium nucleatum* potentiates intestinal tumorigenesis and modulates the tumor-immune microenvironment. *Cell Host Microbe* **14**, 207–215 (2013).
32. Yu, T. et al. *Fusobacterium nucleatum* promotes chemoresistance to colorectal cancer by modulating autophagy. *Cell* **170**, 548–563 (2017).
33. Tomkovich, S. et al. Locoregional effects of microbiota in a preclinical model of colon carcinogenesis. *Cancer Res.* **77**, 2620–2632 (2017).
34. Suzuki, A. et al. CIS3/SOCS3/SSI3 plays a negative regulatory role in STAT3 activation and intestinal inflammation. *J. Exp. Med.* **193**, 471–481. (2001).
35. Li, Y. et al. Disease-related expression of the IL6/STAT3/SOCS3 signalling pathway in ulcerative colitis and ulcerative colitis-related carcinogenesis. *Gut* **59**, 227–235 (2010).
36. Wrigley, J. D. et al. Identification and characterization of dual inhibitors of the USP25/28 deubiquitinating enzyme subfamily. *ACS Chem. Biol.* **12**, 3113–3125 (2017).
37. Parikh, K. et al. Colonic epithelial cell diversity in health and inflammatory bowel disease. *Nature* **567**, 49–55 (2019).
38. Schmitt, M. et al. Paneth cells respond to inflammation and contribute to tissue regeneration by acquiring stem-like features through SCF/c-Kit signaling. *Cell Rep.* **24**, 2312–2328 (2018).
39. Adolph, T. E., Mayr, L., Grabherr, F. & Tilg, H. Paneth cells and their antimicrobials in intestinal immunity. *Curr. Pharm. Des.* **24**, 1121–1129 (2018).
40. Price, A. E. et al. A map of Toll-like receptor expression in the intestinal epithelium reveals distinct spatial, cell type-specific, and temporal patterns. *Immunity* **49**, 560–575 (2018).
41. Bersudsky, M. et al. Non-redundant properties of IL-1 α and IL-1 β during acute colon inflammation in mice. *Gut* **63**, 598–609 (2014).
42. Hasegawa, M. et al. Protective role of commensals against *Clostridium difficile* infection via an IL-1 β -mediated positive-feedback loop. *J. Immunol.* **189**, 3085–3091 (2012).
43. Gao, S. J. et al. Interleukin-18 genetic polymorphisms contribute differentially to the susceptibility to Crohn's disease. *World J. Gastroentero.* **21**, 8711–8722 (2015).
44. Harrison, O. J. et al. Epithelial-derived IL-18 regulates Th17 cell differentiation and Foxp3(+) Treg cell function in the intestine. *Mucosal Immunol.* **8**, 1226–1236 (2015).
45. Tak, T., Tesselaar, K., Pillay, J., Borghans, J. A. & Koenderman, L. What's your age again? Determination of human neutrophil half-lives revisited. *J. Leukoc. Biol.* **94**, 595–601 (2013).
46. Sylvia, C. J. The role of neutrophil apoptosis in influencing tissue repair. *J. Wound Care* **12**, 13–16 (2003).
47. Hart, J. Inflammation. 1: its role in the healing of acute wounds. *J. Wound Care* **11**, 205–209 (2002).
48. Zhao, J., Kim, K. A. & Abo, A. Tipping the balance: modulating the Wnt pathway for tissue repair. *Trends Biotechnol.* **27**, 131–136 (2009).
49. Bradford, E. M. et al. Epithelial TNF receptor signaling promotes mucosal repair in inflammatory bowel disease. *J. Immunol.* **199**, 1886–1897 (2017).
50. Isomoto, H. et al. Sustained IL-6/STAT-3 signaling in cholangiocarcinoma cells due to SOCS-3 epigenetic silencing. *Gastroenterology* **132**, 384–396 (2007).
51. Carow, B. & Rottenberg, M. E. SOCS3, a major regulator of infection and inflammation. *Front. Immunol.* **5**, 58 (2014).
52. Brennan, C. A. & Garrett, W. S. Gut microbiota, inflammation, and colorectal cancer. *Annu. Rev. Microbiol.* **70**, 395–411 (2016).
53. Zhong, B. et al. Negative regulation of IL-17-mediated signaling and inflammation by the ubiquitin-specific protease USP25. *Nat. Immunol.* **13**, 1110–1117 (2012).
54. Zhao, Y. et al. USP2a supports metastasis by tuning TGF- β signaling. *Cell Rep.* **22**, 2442–2454 (2018).
55. Yang, X. O. et al. Regulation of inflammatory responses by IL-17E. *J. Exp. Med.* **205**, 1063–1075 (2008).
56. Li, S. et al. Pathogen blocks host death receptor signalling by arginine GlcNAcylation of death domains. *Nature* **501**, 242–246 (2013).
57. Zhang, M. et al. USP18 recruits USP20 to promote innate antiviral response through deubiquitinating STING/MITA. *Cell Res.* **26**, 1302–1319 (2016).
58. Liuyu, T. et al. Induction of OTUD4 by viral infection promotes antiviral responses through deubiquitinating and stabilizing MAVS. *Cell Res.* **29**, 67–79 (2019).

Acknowledgements

We thank Y. Pan (Fourth Military Medical University) for valuable suggestions, S. Li (Huazhong Agricultural University) for reagents and technical help and members of the Zhong laboratory and the core facilities of the Medical Research Institute for technical help. This study was supported by grants from the National Key Research and Development Program of China (2018TFE0204500 and 2018YFC1004601), National Science Foundation of China (31671454 and 31930040), Fundamental Research Funds for Central Universities (2042020kf0207 and 2042020kf0042), National Science Foundation of Hubei Province (2018CFA016) and Medical Science Advancement Program (Basic Medical Sciences) of Wuhan University (TFJC2018004).

Author contributions

B.Z. designed and supervised the study; X.-M.W. performed the core experiments; C.Y. and Y.Z. helped with mouse breeding and colon cancer modeling; Z.X. and P.W. performed bioinformatics analysis; Z.-G.X., W.Y., D.L. and B.X. collected

CRC samples, produced tissue arrays and performed IHC analysis; J.-Y.F. and C.D. provided reagents; B.Z., X.-M.W. and D.L. wrote the paper; all the authors analyzed data.

Competing interests

The authors declare no competing interests.

Additional information

Extended data is available for this paper at <https://doi.org/10.1038/s43018-020-0089-4>.

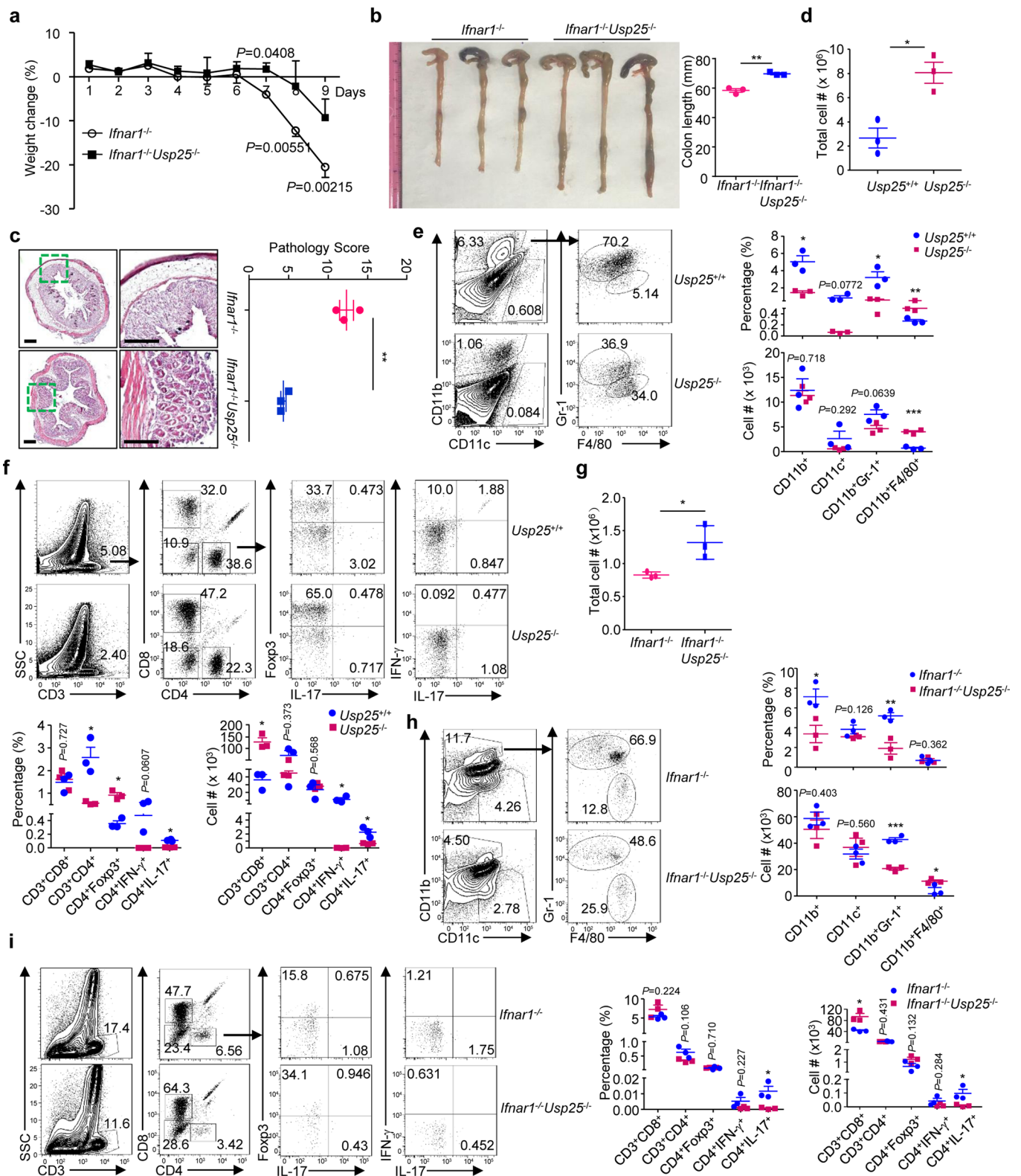
Supplementary information is available for this paper at <https://doi.org/10.1038/s43018-020-0089-4>.

Correspondence and requests for materials should be addressed to B.Z.

Reprints and permissions information is available at www.nature.com/reprints.

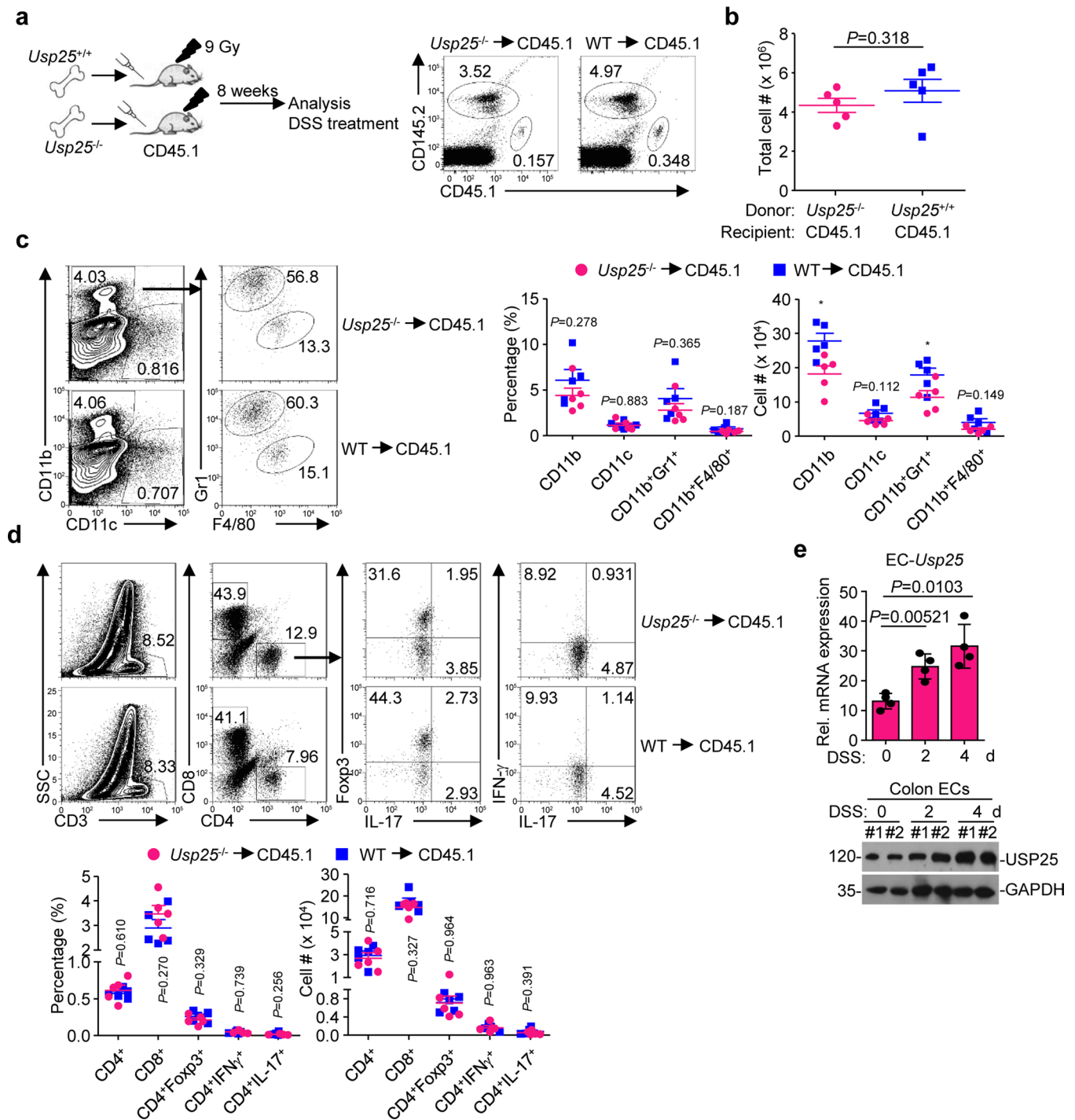
Publisher's note Springer Nature remains neutral with regard to jurisdictional claims in published maps and institutional affiliations.

© The Author(s), under exclusive licence to Springer Nature America, Inc. 2020

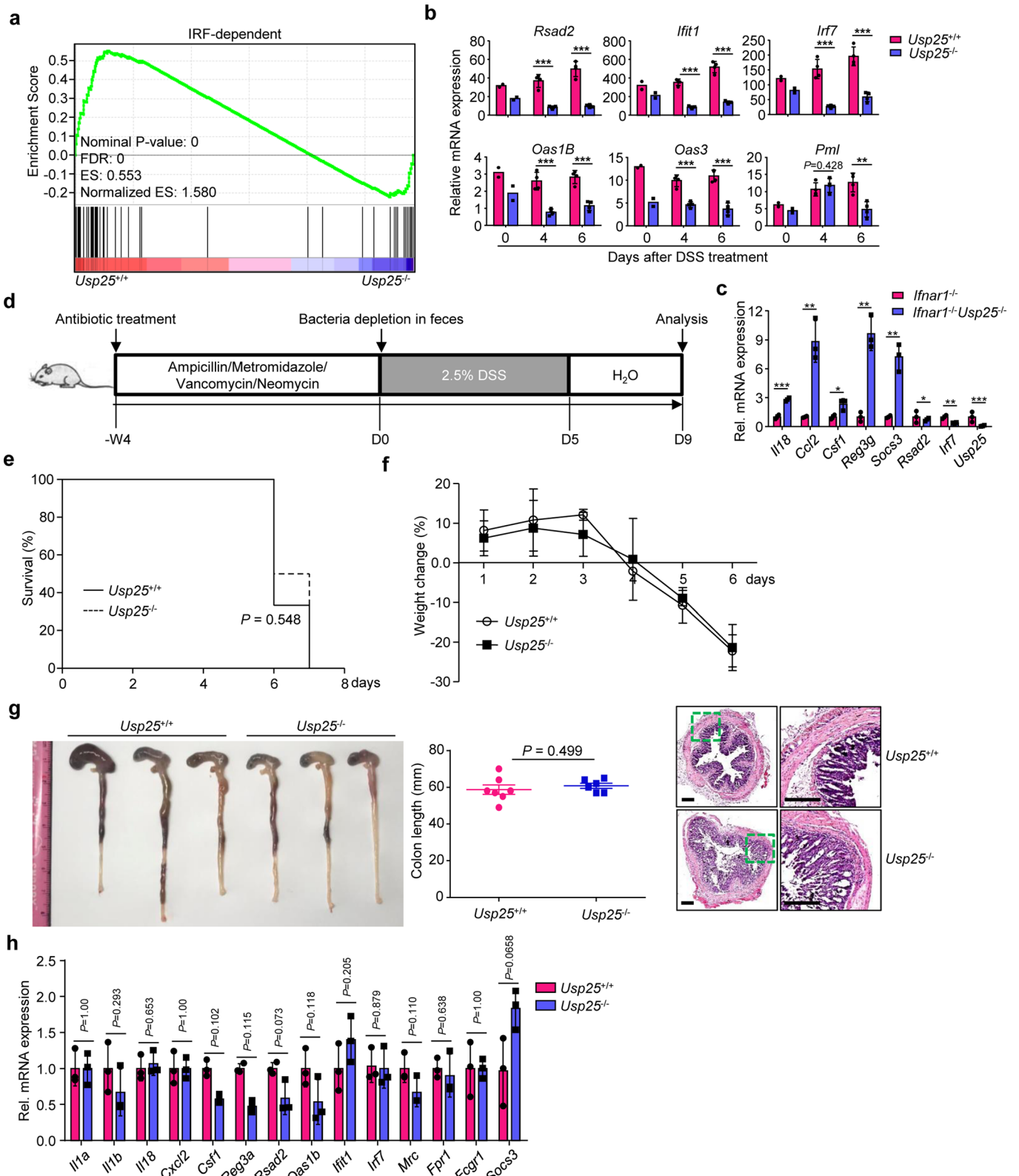


Extended Data Fig. 1 | See next page for caption.

Extended Data Fig. 1 | USP25 deficiency inhibits DSS-induced colitis independently of type I IFN signaling. (a, b) Body weight change (a) and gross morphological change and lengths of colons (b) of *Usp25^{-/-}Ifnar1^{-/-}* mice (n = 3) and *Ifnar1^{-/-}* mice (n = 3) that were given 2% DSS in drinking water for 5 d, followed by normal drinking water for another 4 d. (c) Representative histological images (left) and pathological scores (right) of H&E stained colon sections of *Usp25^{-/-}Ifnar1^{-/-}* mice (n = 3) and *Ifnar1^{-/-}* mice (n = 3) in (a). (d-f) Total cell number (d), representative flow cytometry images and analysis of the percentages and cell number of neutrophils (CD11b⁺Gr-1⁺) and macrophages (CD11b⁺F4/80⁺) (e), CD8⁺, CD4⁺, CD3⁺CD4⁺IFN γ ⁺, CD3⁺CD4⁺IL-17 γ ⁺, and CD3⁺CD4⁺Foxp3⁺ cells (f) from lamina propria in *Usp25^{+/+}* (n = 3) and *Usp25^{-/-}* (n = 3) mice that were given 2.5% DSS in drinking water for 5 d, followed by normal drinking water for another 3 d. (g-i) Total cell number (g), representative flow cytometry images and analysis of the percentages and cell number of neutrophil (CD11b⁺Gr-1⁺) and macrophage (CD11b⁺F4/80⁺) (h), CD8⁺, CD4⁺, CD3⁺CD4⁺IFN γ ⁺, CD3⁺CD4⁺IL-17 γ ⁺, and CD3⁺CD4⁺Foxp3⁺ cells (i) of lamina propria from *Usp25^{-/-}Ifnar1^{-/-}* mice (n = 3) and *Ifnar1^{-/-}* mice (n = 3) that were given 2% DSS in drinking water for 5 d, followed by normal drinking water for another 3 d. **P* < 0.05; ***P* < 0.01 (two-tailed student's *t*-test). Scale bars represent 0.4 mm. Data are representative of two independent experiments (Graphs show mean \pm S.D.). Numerical source data for the experiments in this figure can be found in Numerical_Source_Data_Extended_Data_Fig1.

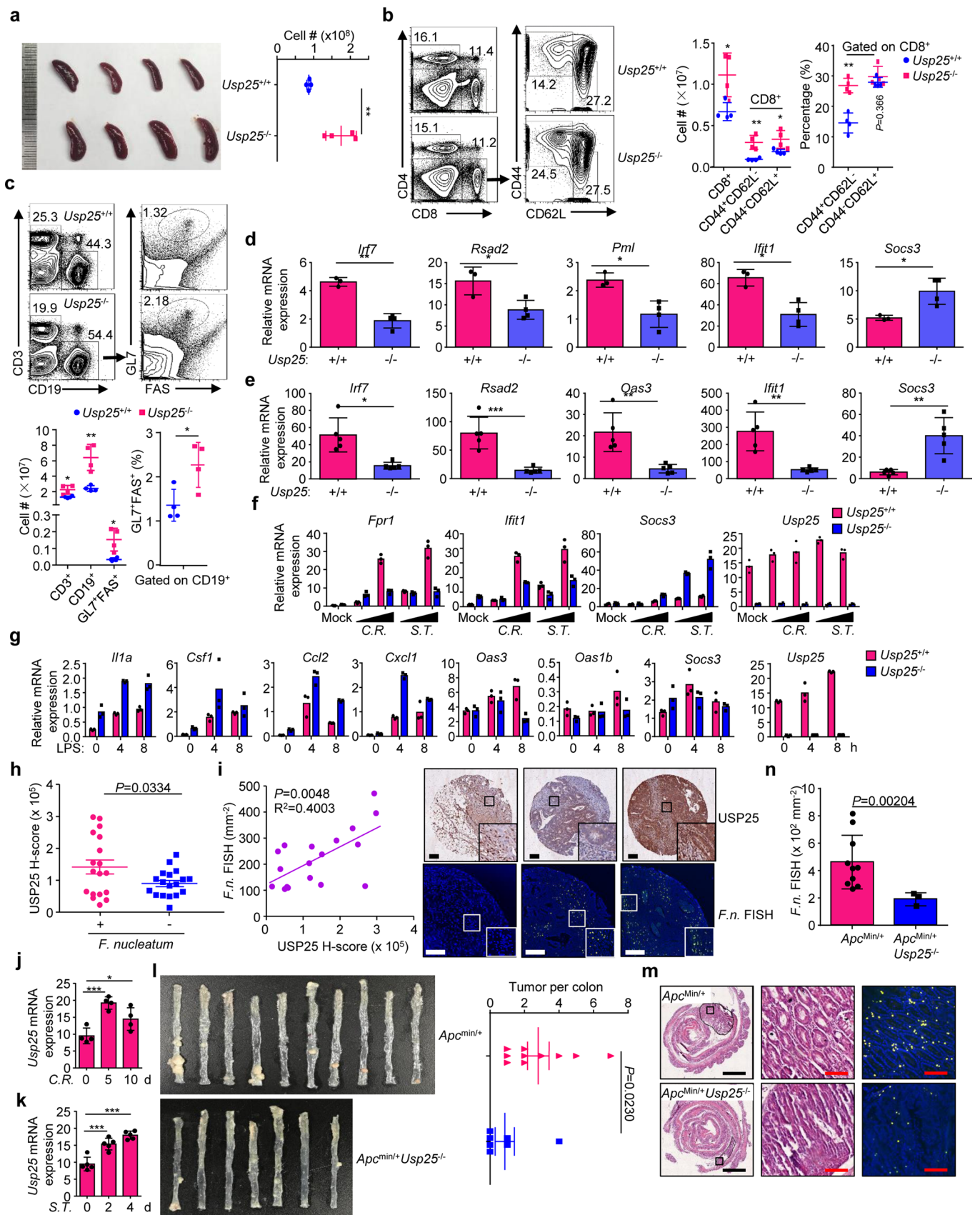


Extended Data Fig. 2 | USP25 deficiency in hematopoietic cells does not affect immune cell homeostasis or differentiation in the colon lamina propria after DSS treatment. (a) Flow cytometry analysis of the blood from irradiated CD45.1⁺ mice that were adoptively transferred *Usp25*^{+/+} ($n=5$) and *Usp25*^{-/-} ($n=5$) bone marrow cells (1×10^6) (CD45.2⁺) for 6 weeks. (b-d) Total cell number (b), representative flow cytometry images and analysis of the percentages and cell number of neutrophil (CD11b⁺Gr1⁺) and macrophage (CD11b⁺F4/80⁺) (c), CD8⁺, CD4⁺, CD3⁺CD4⁺IFN γ ⁺, and CD3⁺CD4⁺Foxp3⁺ cells (d) of lamina propria from mice in (a) that were given 2.5% DSS in drinking water for 5 d, followed by normal drinking water for another 3 d. (e) qRT-PCR analysis of *Usp25* mRNA levels (left graph) ($n=4$ for each time point) and immunoblot analysis ($n=2$ for each time point) of USP25 protein in colon epithelial cells isolated from wild-type mice treated with 2.5% DSS for 0–4 d. Data are representative of two independent experiments (Graphs show mean \pm S.D., two-tailed student's *t*-test.). Uncropped immunoblot images are shown in Uncropped_gels_Extended_Data_Fig.2. Numerical source data for the experiments in this figure can be found in Numerical_Source_Data_Extended_Data_Fig.2.



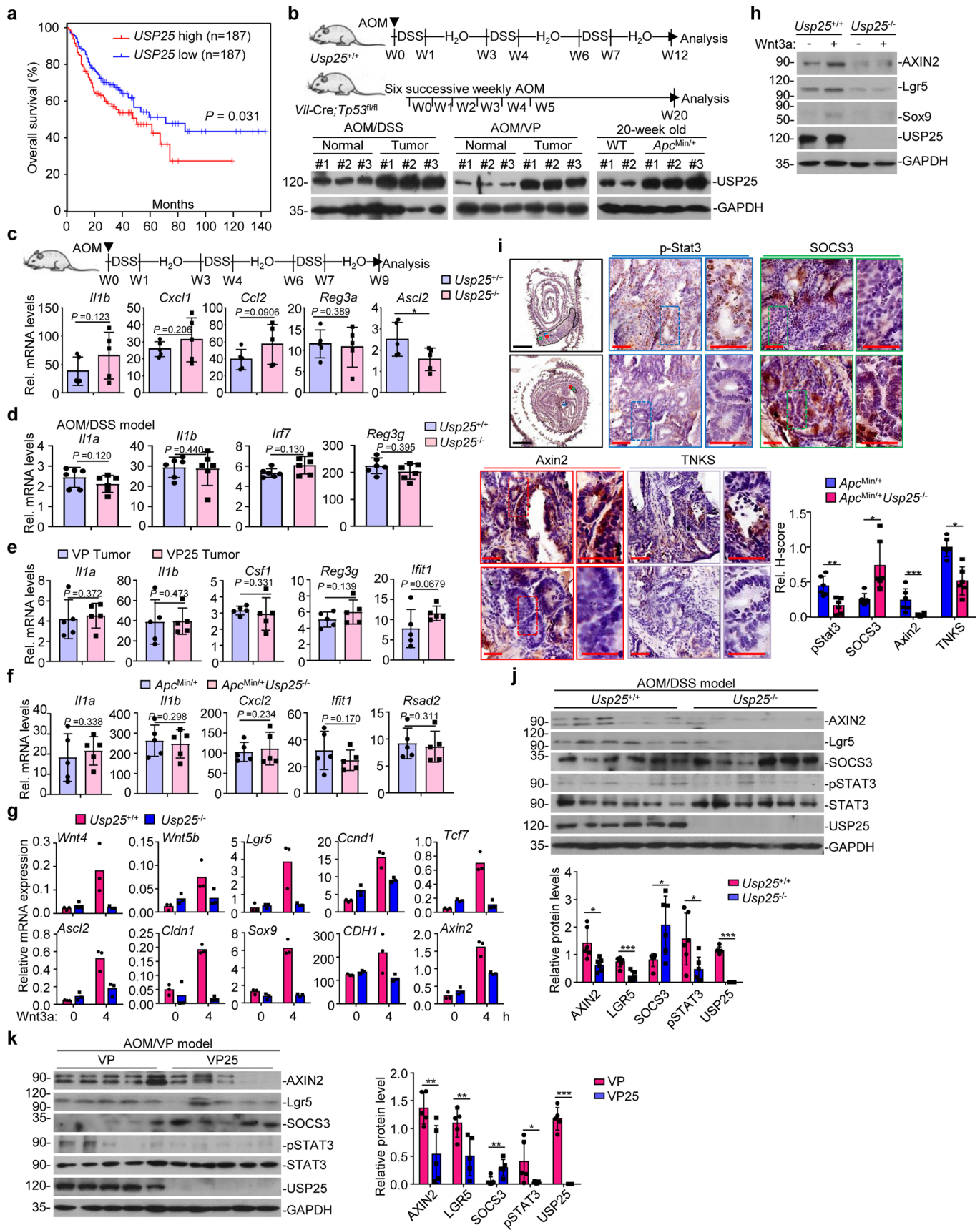
Extended Data Fig. 3 | See next page for caption.

Extended Data Fig. 3 | USP25 deficiency inhibits DSS-induced colitis dependently on gut bacteria. (a) Gene set enrichment analysis of IRF-dependent genes of *Usp25*^{+/+} (n = 2) and *Usp25*^{-/-} (n = 2) mice that were given 2.5% DSS in drinking water for 5 d, followed by normal drinking water for another 2 d. (b) qRT-PCR analysis of IRF-dependent genes in the colons of *Usp25*^{+/+} (n = 2 at day 0, n = 4 at day 4 and 6) and *Usp25*^{-/-} (n = 2 at day 0, n = 4 at day 4 and 6) mice that were given 2.5% DSS in drinking water for 4 or 6 d. (c) qRT-PCR analysis of the indicated genes in the colons from *Usp25*^{-/-}*Ifnar1*^{-/-} (n = 3) and *Ifnar1*^{-/-} (n = 3) mice that were given 2% DSS in drinking water for 5 d, followed by normal drinking water for another 3 d. (d) A scheme of antibiotics treatment and colitis induction. Mice were fed with sterile water containing ampicillin (1 g/L), metronidazole (1 g/L), vancomycin (0.5 g/L), and neomycin (1 g/L). Four weeks later, the mice were used for 2% DSS-colitis analysis. (e) Survival of *Usp25*^{+/+} (n = 6) and *Usp25*^{-/-} (n = 8) mice treated as in (d). (f, g) Body weight change (f), gross morphological change and lengths of colons, and representative H&E stained colon sections (g) of *Usp25*^{+/+} (n = 7) and *Usp25*^{-/-} (n = 6) mice that were treated as in (d). (h) qRT-PCR analysis of the indicated genes in the colons of *Usp25*^{+/+} (n = 3) and *Usp25*^{-/-} (n = 3) mice that were treated as in (d). **P* < 0.05; ***P* < 0.01; ****P* < 0.001 (two-tailed student's *t*-test). Scale bars represent 0.4 mm. Data are representative of two (b, c, h) and combined two (e-g) independent experiments (Graphs show mean ± S.D.). Numerical source data for the experiments in this figure can be found in Numerical_Source_Data_Extended_Data_Fig.3.



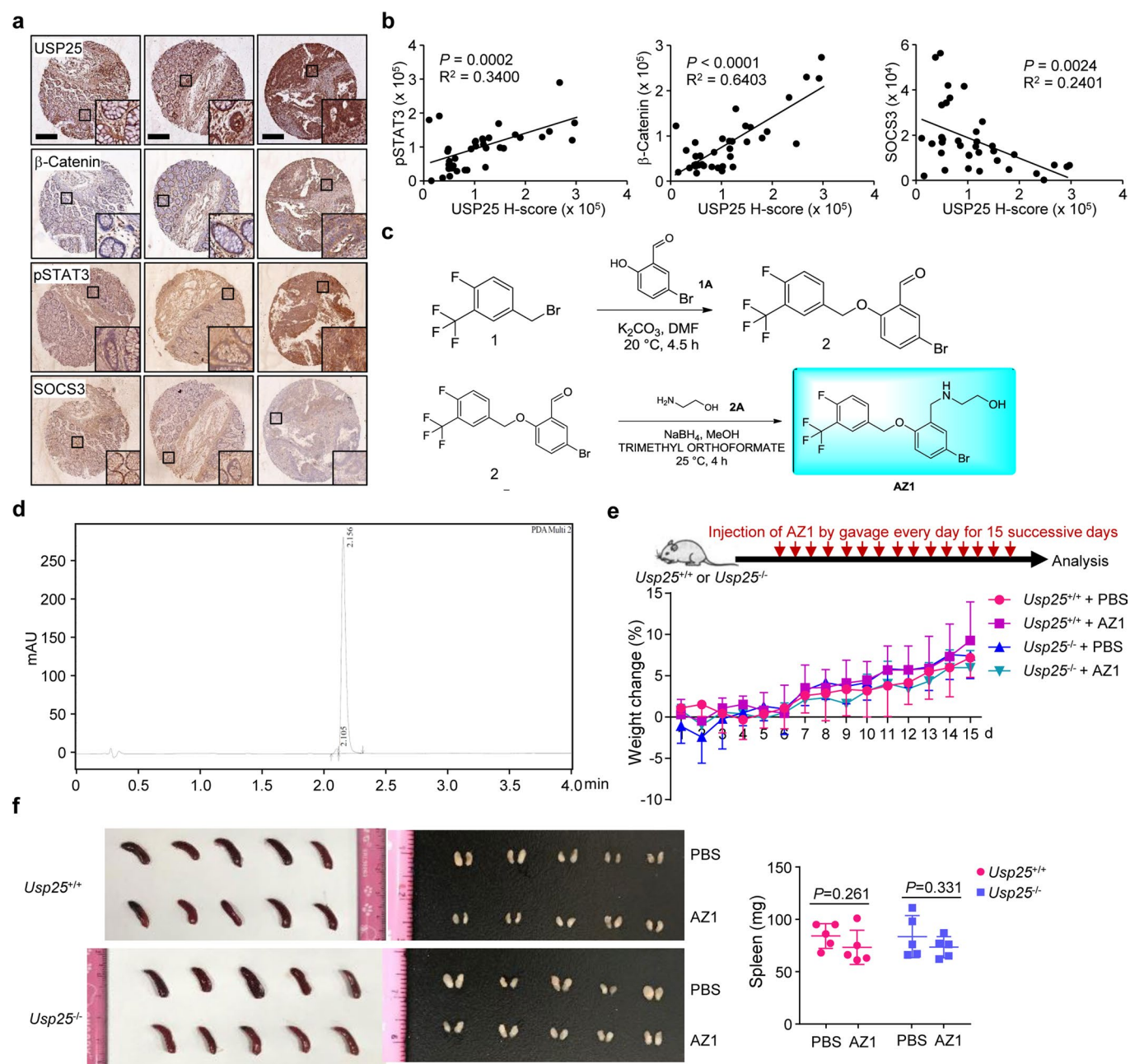
Extended Data Fig. 4 | See next page for caption.

Extended Data Fig. 4 | USP25 deficiency potentiates bacterial infection-induced expression of cytokines. (a) Image (left) and cell number (right) of spleens from *Usp25^{+/+}* (n = 4) and *Usp25^{-/-}* (n = 4) mice that were orally infected with *C rodentium* (1×10^9 CFU) for 14 days. (b, c) Flow cytometry analysis of spleenocytes strained with fluorescence-conjugated antibodies against the indicated surface from mice in (a) (n = 4). (d, e) qRT-PCR analysis of the expression of the indicated genes in the colons from *Usp25^{+/+}* (n = 3) and *Usp25^{-/-}* (n = 3) mice that were orally infected with *C rodentium* (1×10^9 CFU) for 14 days (d) (n = 3 for *Usp25^{+/+}*; n = 4 for *Usp25^{-/-}*) or *S typhimurium* (1×10^7 CFU) for 6 days (e) (n = 5). (f, g) qRT-PCR analysis of the expression of the indicated genes in *Usp25^{+/+}* and *Usp25^{-/-}* colon organoids (n = 3, technical replicates) that were infected with *C rodentium* and *S typhimurium* (CFU of 5×10^6 or 1×10^7) for 1 h (f) or stimulated with LPS (10 mg/ml) for 0–8 h (g). (h) Immunohistochemistry analysis (IHC) of USP25 and fluorescent in situ hybridization (FISH) of *F. nucleatum* in human colorectal cancer tissues (n = 18 for the + or - groups). (i) Correlation analysis (left) and representative images (right) of USP25 protein levels (IHC) and *F. nucleatum* colonization (FISH) in CRC tissues (n = 18). Scale bars represent 0.2 mm. (j) qRT-PCR analysis of the expression of USP25 in the colons from *Usp25^{+/+}* mice day (n = 4 for each time point) that were orally infected with *C rodentium* (1×10^9 CFU) at 0, 5, 10 day. (k) qRT-PCR analysis of the expression of USP25 in the colons from *Usp25^{+/+}* mice day (n = 4 for each time point) that were orally infected *S typhimurium* (1×10^7 CFU) at 0, 2, 4. (l) Representative images and tumor counts of colons from *Apc^{Min/+}* (n = 10) and *Apc^{Min/+} Usp25^{-/-}* (n = 7) mice that were daily fed with *F. nucleatum* (1×10^8 CFU) for 8 weeks beginning at 6 weeks of age. (m, n) FISH (m) and statistical (n) (n = 10 mice for *Apc^{Min/+}*; n = 3 mice for *Apc^{Min/+} Usp25^{-/-}*) analysis of *F. nucleatum* of colon tumors from mice in (l). Black scale bars represent 2 mm. Red scale bars represent 0.1 mm. * $P < 0.05$; ** $P < 0.01$; *** $P < 0.001$ (two-way ANOVA for j and k; two-tailed student's *t*-test for a–e, h, l and n). Data are representative of two independent experiments (Graphs show mean in f and g or mean \pm S.D. in a–e, h, j–n). Numerical source data for the experiments in this figure can be found in Numerical_Source_Data_Extended_Data_Fig.4.

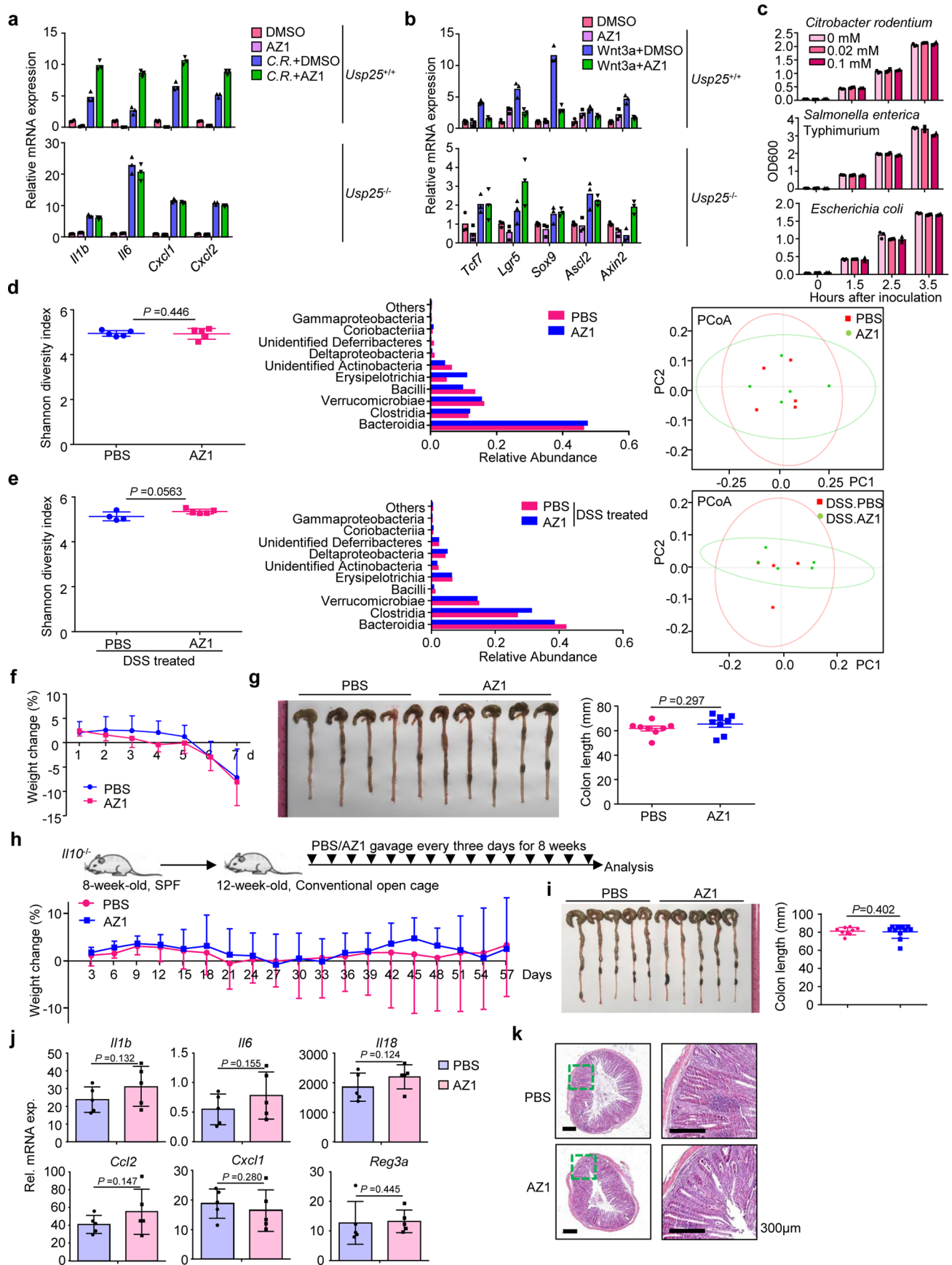


Extended Data Fig. 5 | See next page for caption.

Extended Data Fig. 5 | Negative correlation of USP25 expression level and prognosis of gastrointestinal cancers. (a) The correlation of *USP25* transcript expression with overall survival in gastrointestinal cancer patients (n = 187 for *USP25* high and low patients, GEPIA database). (b) Immunoblot analysis of *USP25* in the colon tumors from *Usp25*^{+/+} mice after AOM/DSS induction for 12 weeks (left), *Vil-Cre;Trp53*^{fl/fl} mice at the 20th week after the first AOM injection (middle), or *Apc*^{Min/+} mice at 20-week-old (right). (c) qRT-PCR analysis of the expression of the indicated genes in the colon from *Usp25*^{+/+} (n = 5) and *Usp25*^{-/-} (n = 5) mice after AOM/DSS induction for 9 weeks. (d-f) qRT-PCR analysis of the expression of the indicated genes in the colon tumors from *Usp25*^{+/+} (n = 5) and *Usp25*^{-/-} (n = 5) mice after AOM/DSS induction (d), *Vil-Cre;Trp53*^{fl/fl} (n = 6) and *Vil-Cre;Trp53*^{fl/fl}*Usp25*^{-/-} (n = 6) mice at the 18th week after the first AOM injection (e), or *Apc*^{Min/+} (n = 5) and *Apc*^{Min/+}*Usp25*^{-/-} (n = 5) mice at 5-month-old (f). (g) qRT-PCR of the Wnt signaling genes in the *Usp25*^{+/+} (n = 3, technical replicates) and *Usp25*^{-/-} (n = 3, technical replicates) colon organoids stimulated with Wnt3a (50 ng/ml) for 4 h. (h) Immunoblot analysis of the indicated proteins in *Usp25*^{+/+} (n = 3, technical replicates) and *Usp25*^{-/-} (n = 3, technical replicates) colon organoids that were left untreated or stimulated with Wnt3a (50 ng/ml) for 4 h. (i) IHC images and the intensity quantification of Axin2, SOCS3, pStat3 and TNKS proteins in small intestine tumors from *Apc*^{Min/+} (n = 6) and *Apc*^{Min/+}*Usp25*^{-/-} (n = 6) mice at 5-month-old. (j, k) Immunoblot analysis and the intensity quantification of the indicated proteins in tumors from *Usp25*^{+/+} (n = 6) and *Usp25*^{-/-} (n = 6) mice after AOM/DSS induction (j), or *Vil-Cre;Trp53*^{fl/fl} (n = 5) and *Vil-Cre;Trp53*^{fl/fl}*Usp25*^{-/-} (n = 5) mice at the 18th week after the first AOM injection (k). **P* < 0.05; ***P* < 0.01; ****P* < 0.001 (two-way ANOVA for g; two-tailed student's *t*-test for c-f, i, j, k). Red and black scale bars represent 50 mm and 1 mm, respectively. Data are representative of at least three independent experiments (Graphs show mean in g or mean ± S.D. in c-f and i-k). Uncropped immunoblot images are shown in `Uncropped_gels_Extended_Data_Fig.5`. Numerical source data for the experiments in this figure can be found in `Numerical_Source_Data_Extended_Data_Fig.5`.

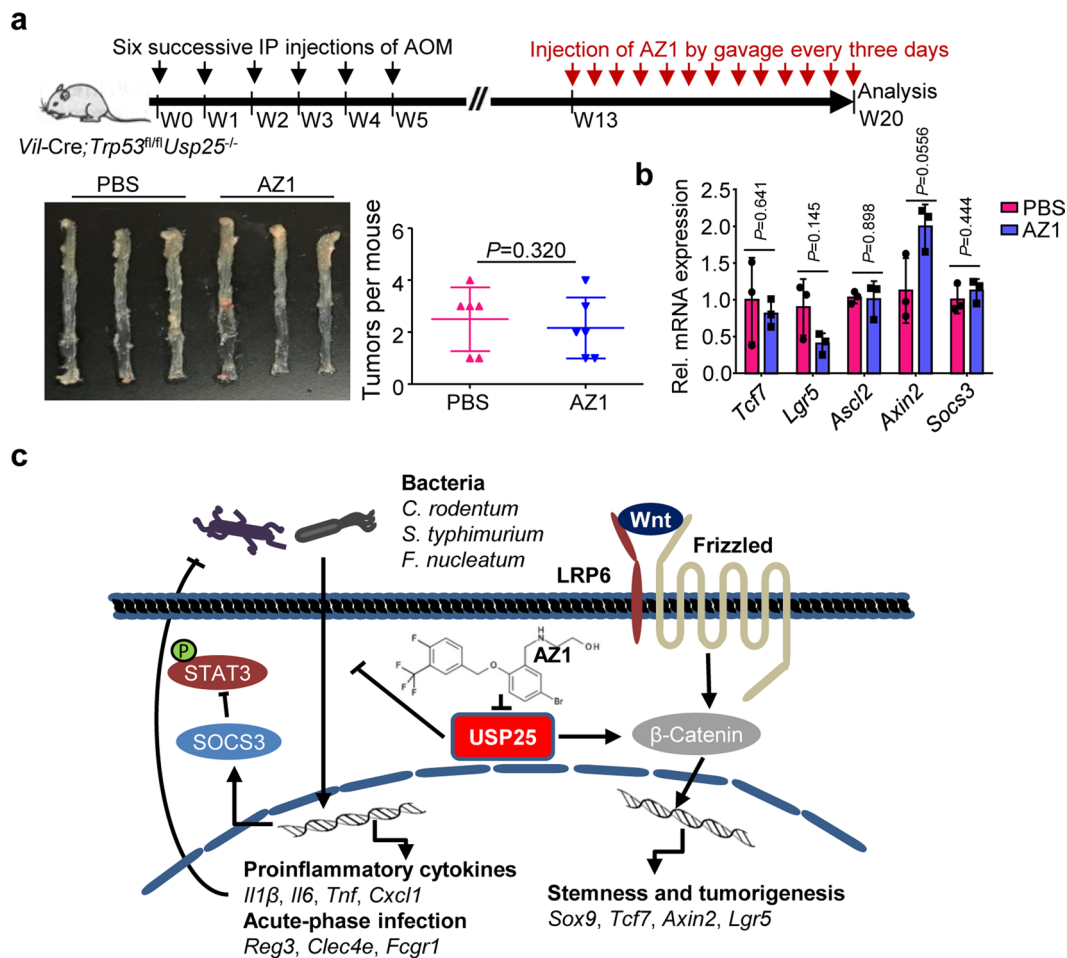


Extended Data Fig. 6 | Synthesis and toxicity analysis of AZ1. (a, b) IHC images of USP25, b-Catenin, SOCS3 and pSTAT3 proteins (a) in patient CRC tissues ($n = 36$) and correlation analysis of USP25 with b-Catenin, SOCS3 and pSTAT3 proteins expression level (b). (c, d) The synthetic method (c) and HPLC chromatography (d) of the inhibitor AZ1. (e, f) Weight change (e) and images of spleens and lymph nodes (f) of 7-week-old male *Usp25^{+/+}* ($n = 5$) and *Usp25^{-/-}* ($n = 5$) mice that were daily injected of PBS or AZ1 (40 mg/kg body weight) by gavage. Scale bars represent 0.4 mm. Data are representative of two experiments (a, e, f) (Graphs show mean \pm S.D., two-tailed student's *t*-test). Numerical source data for the experiments in this figure can be found in Numerical_Source_Data_Extended_Data_Fig.6.



Extended Data Fig. 7 | See next page for caption.

Extended Data Fig. 7 | Selectivity analysis of AZ1 on USP25. (a, b) qRT-PCR analysis of the expression of the indicated genes in *Usp25*^{+/+} (n = 3, technical replicates) and *Usp25*^{-/-} (n = 3, technical replicates) colon organoids infected with *C. rodentium* (a) or treated with Wnt3a (50 ng/ml) (b) in the presence or absence of AZ1 (10 mM) stimulation for 4 h. (c) Growth rate (as indicated by the OD600 values) of different bacteria that were inoculated to fresh LB culture medium (1:200) for the indicated time points after overnight culture (n = 3, technical replicates). (d) Shannon diversity (left), bacterial relative abundance (middle) and PCoA analysis from 16 S rRNA seq in feces of WT mice fed with PBS (n = 5 mice) or AZ1 (n = 5 mice) for 15 days. (e) Shannon diversity (left), bacterial relative abundance (middle) and PCoA analysis from 16 S rRNA seq in feces of WT mice treated by 2.5% DSS for 5 d followed by normal water for 2 d in the presence of PBS (n = 4 mice) or AZ1 (n = 5 mice) by gavage. (f, g) Body weight change (f) and gross morphological change and lengths of colons (g) of *Usp25*^{-/-} mice that were given 2.5% DSS in drinking water for 5 d, followed by normal drinking water for another 2 d in the presence or absence of seven successive daily gavage of PBS (n = 8 mice) or AZ1 (40 mg/kg) (n = 8 mice). (h, i) Weight change (h) and image and colon lengths (i) of *Il10*^{-/-} mice (8-week old) housed in conventional open cage conditions and injected with PBS (n = 9 mice) or AZ1 (40 mg/kg) (n = 11 mice) by gavage every three days starting from 12-week old for 8 successive weeks. (j, k) qRT-PCR of the distal colon tissues (j) (n = 5 mice for PBS and AZ1 groups) and HE staining of colon (k) (PBS, n = 9 mice; AZ1, n = 11 mice) of *Il10*^{-/-} mice treated as in (h). **P* < 0.05; ***P* < 0.01; ****P* < 0.001. (two-tailed Student's *t*-test). Scale bars represent 300 μm. Data are representative of three (a–e) or two (j) independent experiments or combined two independent experiments (f–i) (Graphs show mean in a–c or mean ± S.D. in d–j). Numerical source data for the experiments in this figure can be found in Numerical_Source_Data_Extended_Data_Fig.7.



Extended Data Fig. 8 | AZ1 has minimal effect on colon tumorigenesis in the USP25 deficient background. (a) A scheme of colon tumor induction in *Vil-Cre;Trp53^{fl/fl}Usp25^{-/-}* mice (upper). Representative images and tumor counts of colons from *Vil-Cre;Trp53^{fl/fl}Usp25^{-/-}* mice that were weekly injected with AOM (10 mg/kg) for six successive weeks, followed by injection of PBS ($n=6$ mice) or AZ1 (20 mg/kg) ($n=6$ mice) by gavage every three days from 12th to 18th weeks after initial AOM injection (lower). (b) qRT-PCR of the indicated genes in colon tumors from *Vil-Cre;Trp53^{fl/fl}Usp25^{-/-}* mice treated in (a) ($n=3$ mice for PBS and AZ1 groups). (c) A model for USP25 to modulate colonic infections, inflammations and colon cancer. USP25 inhibits the expression of anti-bacteria genes, promotes bacterial infections and inflammation in the colon, downregulates SOCS3 to facilitate activation of STAT3, and promotes Wnt signaling to increase the stemness of colonic epithelial cells, which are inducers of colon cancer. Pharmacological inhibition of USP25 impairs inflammation, restricts bacterial infections and inhibits tumorigenesis in the colon. Two-tailed student's t-test. Data are combination (a) or representative (b) of two independent experiments (Graph show mean \pm S.D.). Numerical source data for the experiments in this figure can be found in Numerical_Source_Data_Extended_Data_Fig.8.